THESIS

SIMULATION OF ALPINE SNOW DISTRIBUTIONS IN THE NORTHERN COLORADO ROCKY MOUNTAINS USING A NUMERICAL SNOW-TRANSPORT MODEL

Submitted by

Ethan M. Greene

Atmospheric Science

In partial fulfillment of the requirements

for the degree of Master of Science

Colorado State University

Fort Collins, Colorado

Fall 1999

COLORADO STATE UNIVERSITY

September 24, 1999

WE HEREBY RECOMMEND THAT THE THESIS PREPARED UNDER OUR SUPERVISION BY ETHAN M. GREENE ENTITLED SIMULATION OF ALPINE SNOW DISTRIBUTIONS IN THE NORTHERN COLORADO ROCKY MOUNTAINS USING A NUMERICAL SNOW-TRANSPORT MODEL BE ACCEPTED AS FULFILLING IN PART REQUIREMENTS FOR THE DEGREE OF MASTER OF SCIENCE

Committee on Graduate Work

Committee Member

Committee Member

Committee Member

Adviser

Department Head

ABSTRACT OF THESIS

SIMULATION OF ALPINE SNOW DISTRIBUTIONS IN THE NORTHERN COLORADO ROCKY MOUNTAINS USING A NUMERICAL SNOW-TRANSPORT MODEL

Two methodologies for simulating winter snow distributions in alpine terrain are presented. First, a numerical snow-transport model (SnowTran-3D) is driven from direct meteorological observations, and second, SnowTran-3D is driven from a regional atmospheric model (ClimRAMS). In each case the simulated snow distributions are compared to observed snow depth transects within two alpine sites in the Northern Colorado Rocky Mountains, Rocky Mountain National Park, and Medicine Bow Mountains. The atmospheric conditions at these sites are characterized by persistent westerly winds with average speeds of 13 m/s, which is significantly greater than the threshold for snow transport (approximately 5 m/s). Consequently, snow redistribution by wind is the dominate component in this environment. Drift features in these areas form around rocks, alpine vegetation, and small and large topographic variations. The model successfully simulated the large-scale snow drifts, but due to the relatively coarse resolution of the vegetation and topographic data inputs (30 m), the model was unable to reproduce some of the smaller scale snow drift features. The model built large drifts in the upper regions of the east facing cirques in Rocky Mountain National Park, in regions where large perennial snow fields are observed. The model results support the theory that snow transport by wind is an important factor in sustaining these snow fields.

Ethan M. Greene
Atmospheric Science
Colorado State University
Fort Collins, Colorado 80523
Fall 1999

ACKNOWLEDGEMENTS

During the course of this project I benefited from the assistance and expertise of many individuals. My adviser Dr. Roger Pielke provided me with an environment where I could peruse my own ideas and interests. This project and my learning experience benefited tremendously from his support and advise. Dr. McKee and the Colorado Climate Center provided some of the instrumentation used in this study. Dr. McKee helped me understand both how to observe atmospheric conditions and how to evaluate my observations. Dr. Elder provided equipment for and experience with determining characteristics of seasonal snowcovers. He helped me expand my knowledge of the many physical processes which affect snowcovers and their seasonal cycles.

I could never have completed this project without the constant patience and assistance of Dr. Glen Liston. Dr. Liston's expertise in both modeling and field research was invaluable during the course of this study. He was able to guide me through this project, constantly keeping me on track while always allowing me to develop my own ideas. Under his guidance I have been able to experience both the strengths and weaknesses of modeling and observational science. He helped me develop a more comprehensive view of snow science.

This research was supported by grant No. NA67RJ0152 from the National Oceanographic and Aeronautical Administration (NOAA) entitled "Parameterizing Subgrid-Scale Snow-Cover Heterogeneities for Use in Regional and Global Climate Models". The meteorological instrumentation was lent to me by Dr. William Malm of the National Park Service Air Resources Division and Air Resource Specialists (ARS). Roger Tree from ARS helped me program the CR-10. Terry Flint and Walt Naylor from the Atmospheric Science Department helped me acquire and build the meteorological tower and mounting systems. Dallas McDonald helped edit and format the final document.

Last but certainly not least, I would like to thank my family for their constant support and encouragement. Most of all my constant companion Dana Trenary. She has always had more confidence in me than I have in myself. Without her unconditional love and support I would have never made it this far.

TABLE OF CONTENTS

LIST OF FIGURES

LIST OF TABLES

Chapter 1

INTRODUCTION AND PREVIOUS WORK

1.1 Introduction

The redistribution of snow by wind is a major contributing factor to the spatial and temporal distribution of seasonal snowcovers. In alpine environments it is a dominant force behind the distribution of snow (Balk and Elder 2000; Billings 1973; Daly 1984; Elder et al. 1991), and also plays a key role in determining the amount of snowcover returned to the atmosphere by sublimation (Schmidt 1972, 1991). Hence, the physical processes associated with blowing and drifting snow are of importance to a wide scope of disciplines. The ability to accurately simulate or predict snow redistribution by wind can improve spring runoff predictions in terms of both magnitude and spatial variability, especially in areas where snow has been blown into a neighboring drainage catchment (Luce et al. 1998). Redistribution of snow also affects the spatial distribution of early-season soil moisture which can directly influence agriculture production (Olienyk 1979), and alpine vegetation germination and growth (Evans et al. 1989; Walker et al. 1993). Reliable calculations of snow-mass redistribution by wind into avalanche-path starting zones would allow more accurate avalanche stability predictions, assisting avalanche forecasters in their efforts to safeguard highways and ski areas, and provide stability information for backcountry areas (Perla 1970; LaChapelle 1980; Buser et al. 1985; Schmidt and Hartman 1986; Ferguson et al. 1990; McClung and Schaerer 1993; Birkeland 1997). Improvements in our understanding and ability to simulate the erosion and deposition of seasonal snow are expected to assist advancements in hydrology, agriculture, and avalanche forecasting and safety. In the current study, the three-dimensional snow-transport model (SnowTran-3D) developed by Liston and Sturm (1998) is applied to two alpine sites in Colorado.

The central feature of each study area are regions above treeline and north/south running ridgelines. Atmospheric forcing inputs for the SnowTran-3D simulations are provided by, 1) meteorological observations, and 2) output from a regional climate model. In each case the modeled snowdrift distribution is compared to the observed snow distribution.

The objective of this study is to evaluate our ability to simulate the physical processes which govern the distribution of seasonal snow in an alpine environment. To accomplish this we will use a numerical snow-transport model which has been shown to adequately simulate these processes in an Arctic environment (Liston and Sturm 1998). We will also examine the simulated snow distribution when the snow-transport model is driven with 1) direct meteorological observations, and 2) atmospheric fields generated by a regional atmospheric modeling system. In each case, available atmospheric data are used to guide the modeling portion of the study. Snow depth observations are observed along linear transects over varying terrain and used as validation for the model results.

1.2 Previous Work

There have been many previous efforts to model snowdrift formation. Many of these efforts have approached this process as a two-dimensional problem (Berg and Caine 1975; Tabler 1975; Berg 1986; Uematsu et al. 1989; Liston et al. 1993; Sundsbø 1997, Naaim et al. 1998). These studies examined snow transport over a barrier, creating snow-distribution profiles on the windward and lee sides of the barrier. Moore et al. (1994) used a two-dimensional model to study how snow drifting occurred around buildings in the Antarctic. The Prairie Blowing Snow Model (Pomeroy et al. 1993) included important processes such as sublimation in a blowing snow model capable of simulating equilibrium transport under steady-state conditions. Fewer studies have attempted to model the three-dimensional distribution of snow deposited by wind. Using a model which computed the air flow and predicted snowdrift rates, Uematsu (1993) simulated snowdrifts over a level surface, and Uematsu et al. (1991) simulated wind-flow patterns and snow distributions around a small building and small hill. Pomeroy et al. (1997) modified the Prairie Blowing Snow Model for use in the Arctic. Their study utilized a vegetation data set

which defined areas as either sources or sinks of blowing snow. The model was driven by monthly-mean climatological data and produced an end-of-winter snow distribution. A rule- and cell-based model of snow transport and distribution has also been applied to a three-dimensional snow-distribution problem in Scotland (Purves et al. 1998). Gauer (1998) used a three-dimensional numerical model to simulate snow-transport processes at an alpine site in Switzerland. The snow-transport model contains two layers. The mass concentrations with the turbulent suspension layer and saltation layer are computed and interactions between the two are accounted for. The Navier-Stokes equations are solved to compute the wind field and the model accounts for the mass-concentration increase of airborne snow due to particle ejection. Liston and Sturm (1998) developed and used a model to reproduce the three-dimensional, wind-modified snow distribution in Arctic Alaska. This model performed well for a site which included complex terrain devoid of trees. Previous researchers have used data from one or more meteorological stations to drive their snow-transport model. In Chapter 3 a similar methodology is followed. In Chapter 4 the output from an atmospheric modeling system is used to drive the snow-transport model.

Chapter 2

MODEL DESCRIPTION

2.1 SnowTran-3D

SnowTran-3D was developed to simulate blowing snow processes in complex terrain (Liston and Sturm 1998). The snow-transport model is fully three-dimensional, in that it is implemented in two horizontal dimensions (x and y), and evolves the snow and snow-water-equivalent depth (the z dimension) over a topographically-variable domain. The model considers only transport variations resulting from accelerating and decelerating flow (i.e., convergent and divergent wind fields). The model does not account for non-equilibrium transport due to temporal wind-speed accelerations and decelerations (e.g., transport variations due to turbulent wind fluctuations). The topography within the model domain can vary from flat, to gently rolling, to highly varying, such as regions containing sharp ridges, gullies, or valleys.

Figure 2.1 illustrates the key input parameters (solar radiation, precipitation, wind speed and direction, air temperature, humidity, topography, vegetation snow-holding capacity), the key processes (saltation, turbulent-suspension, sublimation), and the key outputs (spatial distribution of snow erosion and deposition) from the model. The six primary components of the snow-transport model are: 1) the computation of the wind-flow forcing field, 2) the wind-shear stress on the surface, 3) the transport of snow by saltation, 4) the transport of snow by turbulent suspension, 5) the sublimation of saltating and suspended snow, and 6) the accumulation and erosion of snow at the snow surface, a lower boundary that is allowed to move with time.

The foundation of this snow-transport model is a mass-balance equation which describes the temporal variation of snow depth at a point. Deposition and erosion, which

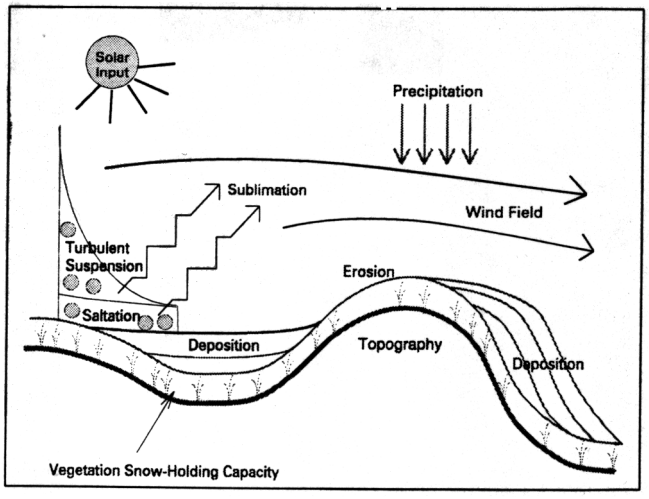

Figure 2.1: Key features of the snow-transport model applied to topographically-variable terrain (from Liston and Sturm 1998).

lead to changes in snow depth at a point are the result of 1) changes in horizontal mass-transport rates of saltation, Q_s (kg m^{-1} s^{-1}); 2) changes in horizontal mass-transport rates of turbulent-suspended snow, Q_t (kg m^{-1} s^{-1}); 3) sublimation of transported snow particles, Q_v (kg m^{-2} s^{-1}); and 4) the water-equivalent precipitation rate, P (m s^{-1}). Combined, the time rate of change of snow depth, ζ (m), is

$$\frac{d\zeta}{dt} = \frac{1}{\rho_s}\left(\rho_w P - \left(\frac{dQ_s}{dx} + \frac{dQ_t}{dx} + \frac{dQ_s}{dy} + \frac{dQ_t}{dy}\right) + Q_v\right) \tag{2.1}$$

where t is time in s, x and y are the horizontal coordinates in m of the west-east and north-south directions, and ρ_s and ρ_w are the snow and water density in kg m^{-3}, respectively. Figure 2.2 provides a schematic of this mass-balance accounting. Equation (2.1) is solved for each individual grid cell within a domain, and is coupled to the neighboring cells through the spatial derivatives $(d/dx, d/dy)$. Complete details of the formulation of each term in Equation (1) can be found in Liston and Sturm (1998).

To drive the snow-transport model, the model requires a reference-level wind-flow field over the domain of interest for each time step. This wind field is generated by taking observed wind speeds and directions, and interpolating them to the model grid. To account for topographic influences, the wind distribution is modified by multiplying by an

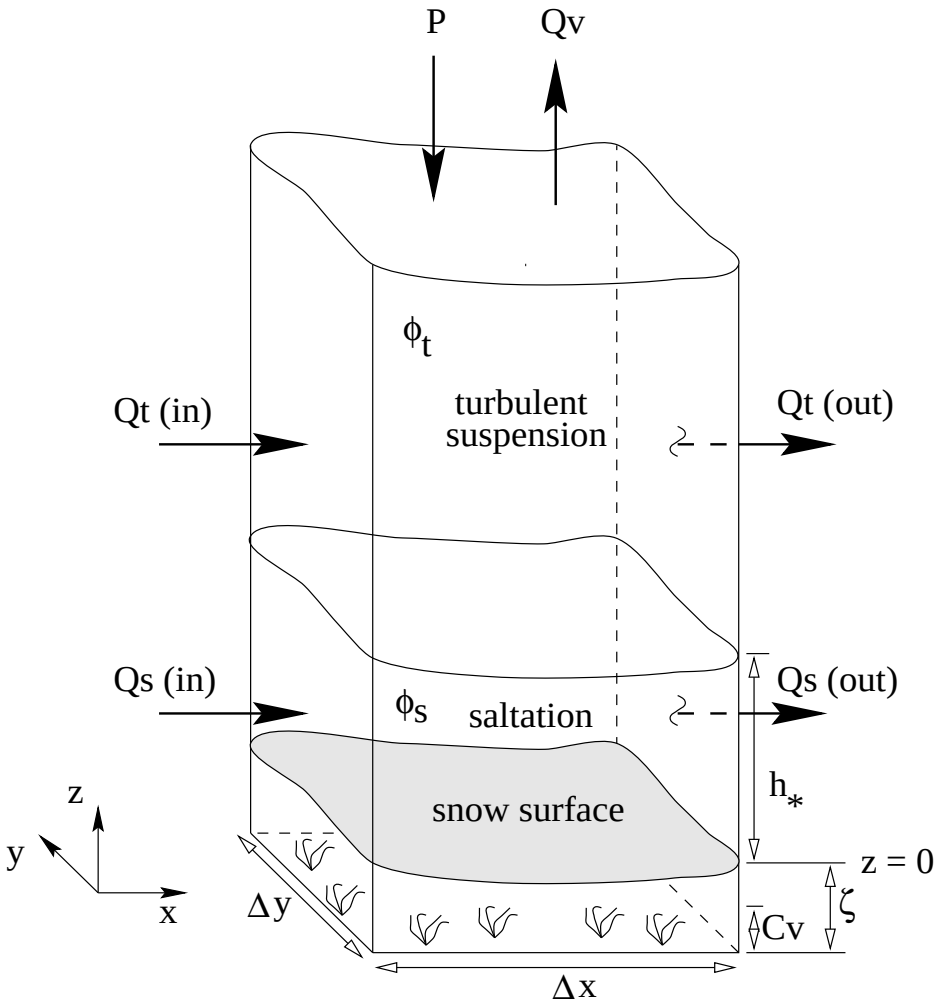

Figure 2.2: Schematic of the SnowTran-3D snow-transport model mass-balance computation (from Liston and Sturm 1998).

empirically-based weighting factor, W,

$$W = 1.0 + \gamma_s \Omega_s + \gamma_c \Omega_c, \tag{2.2}$$

where Ω_s and Ω_c are the topographic slope and curvature, respectively, in the direction of the wind, and γ_s and γ_c are positive constants that weight the relative influence of Ω_s and Ω_c on the wind speed. The slope and curvature are computed such that lee and concave slopes produce Ω_s and Ω_c less than zero, and that windward and convex slopes produce Ω_s and Ω_c greater than zero. Thus, lee and concave slopes produce reduced wind speeds, and windward and convex slopes produce increased wind speeds.

The availability of snow for transport is determined by defining a snow-holding capacity, $C_v(m)$, for each vegetation type or land-surface classification within the domain. This capacity is a function of vegetation height and density. Snow accumulates until the depth exceeds the vegetation snow-holding capacity. Once the snow depth exceeds the capacity, any additional snow is available for transport.

2.2 ClimRAMS

The Regional Atmospheric Modeling System (RAMS) was developed at Colorado State University predominantly to facilitate research into mesoscale and regional, cloud and land-surface atmospheric phenomena and interactions (Pielke 1974; Tripoli and Cotton 1982; Tremback et al. 1985; Pielke et al. 1992; Walko et al. 1995a). This model is fully three-dimensional; nonhydrostatic (Tripoli and Cotton 1980); includes telescoping, interactive nested-grid capabilities (Clark and Farley 1984; Walko et al. 1995b); supports various turbulence closure (Deardorff 1980; McNider and Pielke 1981; Tripoli and Cotton 1986), short and longwave radiation (Mahrer and Pielke 1977; Chen and Cotton 1983, 1987; Harrington 1997), initialization (Tremback 1990), and boundary condition schemes (Pielke et al. 1992); includes a land-surface, energy-balance submodel which accounts for surface fluxes due to vegetation, open water, and snow (Mahrer and Pielke 1977; McCumber and Pielke 1981; Tremback and Kessler 1985; Avissar and Mahrer 1988; Lee 1992; Liston et al. 1999); and includes several cloud microphysical submodels describing liquid

and ice processes related to clouds and precipitation (Meyers et al. 1992; Meyers 1995; Schultz 1995; Walko et al. 1995a). In numerous publications RAMS has been shown to successfully simulate weather processes. For the purposes of this study, multi-month simulations are required. To fulfill that need, a climate version of RAMS (ClimRAMS) has been used (Liston and Pielke 1999)

In order to realistically simulate fall, winter and spring climates the model must account for the effects of seasonal snowcover. Recent additions to ClimRAMS make multi-seasonal simulations possible (Liston and Pielke 1999). In the model, snow accumulates on the ground when the temperature of the lowest layer in the atmospheric model is less than 2°C. The snowcover is represented by one layer of constant density and thermal properties. The surface albedo of the snow is modified depending on whether the snow is dry (albedo = 0.8) or melting (albedo = 0.6) (Gray and Male 1981; Cline 1997); for thin snowcovers (less than 5 cm snow-water equivalent), the albedo changes linearly to the albedo of the underlying surface with decreasing snow depth. Snowcover also modifies the ground heat flux computation and the surface roughness. When the snow melts in the model it contributes directly to the soil moisture. Snow is assumed to fall through the vegetative canopy where it modifies the under-canopy radiation budget; interception by the vegetative canopy is not taken into consideration. Each vegetation type is assigned a characteristic height, and once the snow depth exceeds that height, the surface characteristics become that of snow rather than the vegetation.

The ClimRAMS land-surface scheme includes all the terms required to satisfy a surface energy balance, and the energy available to melt snow is computed within this scheme. Incoming shortwave radiation is a function of time of day and year, and is attenuated as it passes though the atmosphere. Longwave radiation is emitted and absorbed by the atmosphere. The vegetative canopy reduces the amount of radiation incident on the surface below. The longwave fluxes from the vegetated and bare surfaces are a function of the surface temperatures. The latent energy flux is a function of atmospheric pressure, air density, wind speed, and the vapor pressure gradient above the surface. The sensible energy flux is a function of air temperature, stability, wind speed, and the temperature

gradient between the lowest level of the atmosphere and the surface. The surface energy balance is solved to yield the surface temperature. In the presence of snow, surface temperatures greater than 0°C resulting from the surface-energy balance indicate that energy is available for melting. The heat energy available for melting is computed by setting the surface temperature to 0°C and recomputing the surface-energy balance.

Chapter 3

SNOWTRAN-3D FORCED BY METEOROLOGICAL OBSERVATIONS

3.1 Introduction

The first method used to simulate the snow drifting process was to drive SnowTran-3D from direct meteorological observations. During this portion of the study, a weather station was installed near Montgomery Pass, Colorado. The data collected at this site, in combination with SNOTEL data, were used as the atmospheric forcing required by SnowTran-3D. Observations of snow depth taken along a two-dimensional transect were used to evaluate the performance of the model simulation.

3.2 Site Description

Montgomery Pass is situated in an alpine portion of the northern Colorado Rocky Mountains. The pass lies in the Colorado State Forest section of the Medicine Bow Mountains, north of Rocky Mountain National Park and Colorado Highway 14. At an elevation of 3333 m, Montgomery Pass is above treeline and part of a north/south oriented ridgeline (Figure 3.1).

The simulation domain is centered on the ridgeline containing Montgomery Pass. The pass lies near the southern boundary of the domain (Figure 3.2). Elevations within the simulation domain range between 3175 and 3521 meters above sea level. The domain is 2.7 km along the north/south axis, 2.25 km along the east/west axis, and includes dense forest cover on both sides of the ridgeline.

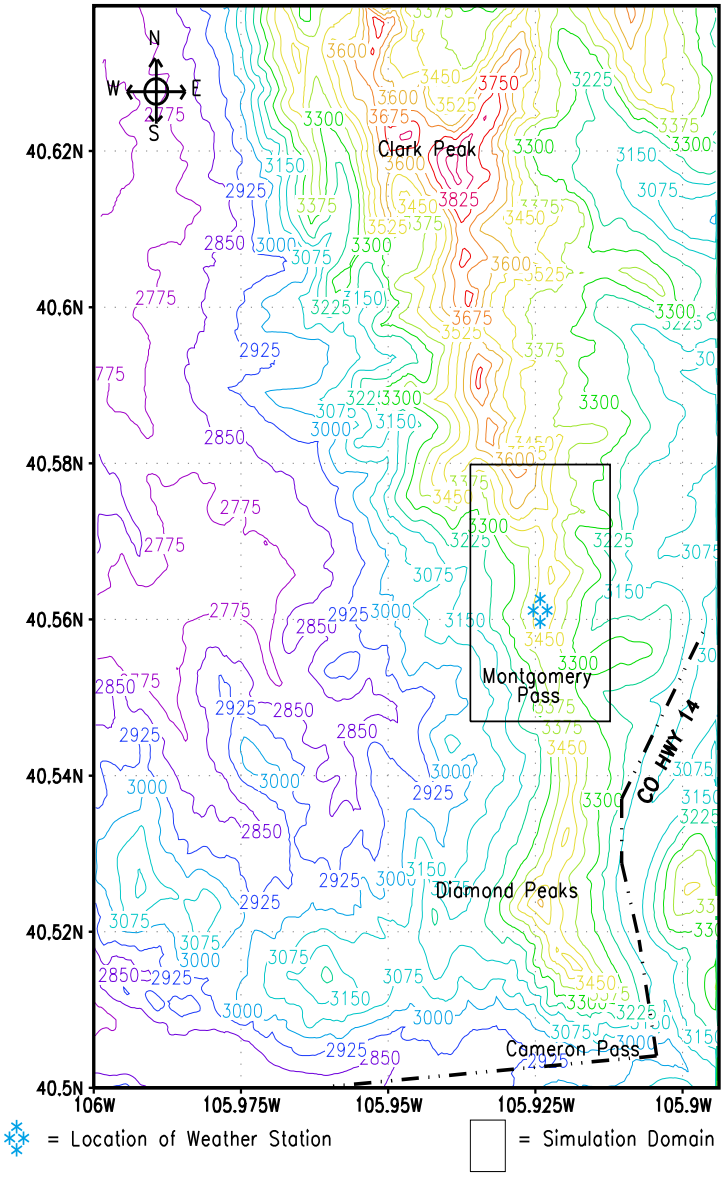

Figure 3.1: USGS 7.5 minute quadrangle for Clark Peak Colorado. Montgomery Pass lies on the main north/south running ridgeline. The Cache La Poudre river drainage lies to the east of the pass, and North Park lies to the west. Contours of elevation appear in 25 m intervals.

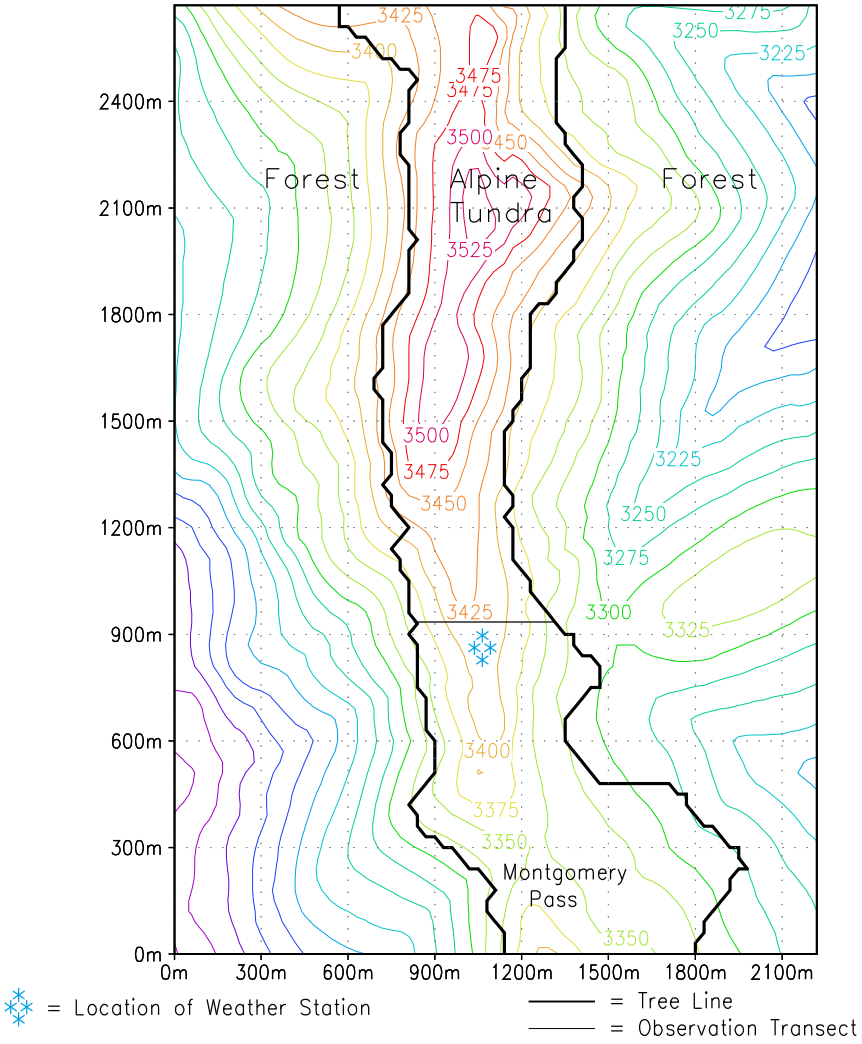

Figure 3.2: Topography and vegetation for the model simulation domain. Contour interval is 25 m. The thick black line indicates treeline which is the division between evergreen forest and alpine tundra. Also shown is the location of the remote weather station and the observation transect.

3.3 Field Procedures

In mid-December 1997, a 3 m tower and instrumentation array were installed on the ridgeline 800 m north of Montgomery Pass (Figure 3.2 and 3.3). The array contained instruments capable of recording air temperature, relative humidity, wind direction, and wind speed. Thirty-minute averages of these observations were recorded on a Campbell CR-10 data logger. The weather station was in place from December 1997 until April 1998. Precipitation measurements were obtained from the snow pillow at the Natural Resources Conservation Service SNOTEL site at Joe Wright. The Joe Wright site lies 4 km to the southeast of the weather station at 3066 m above sea level.

On February 18, 1998 the snow depth was observed along an east/west-running transect. The transect extended from the east treeline to the west treeline and crossed the ridge crest near the weather station site. Using a set of probes marked in 10 cm increments, snow depth measurements were taken at 5 m intervals along this transect (Figure 3.4). These data were used to verify the SnowTran-3D simulations.

3.4 Methodology

For this portion of the study the model used a 30 m grid over the previously-described domain (Figure 3.1). Temporal integrations were computed daily for 56 days. This time period spanned from the installation of the weather station (December 24, 1997), until the snow depth transect was observed (February 18, 1998).

Many studies have shown that precipitation amounts vary with location and elevation in mountainous terrain (Hjermstad 1970; Baopu 1995; Johnson and Hanson 1995; Snook and Pielke 1995; Obleitner and Mayr 1996). The simulations for this study were initially run with the observed precipitation from the Joe Wright SNOTEL site. These simulations produced a snowdrift distribution similar to that observed. However, the modeled drift mass was less than the observed drift mass. In order to compensate for the difference in elevation between the study site and the Joe Wright SNOTEL site, the precipitation was increased until the model-simulated drift mass was within 1% of the observed. This compensation for elevation differences increased the period precipitation by 2%. The

Figure 3.3: The Montgomery Pass Weather Station. Looking west of the Medicine Bow Mountains into North Park.

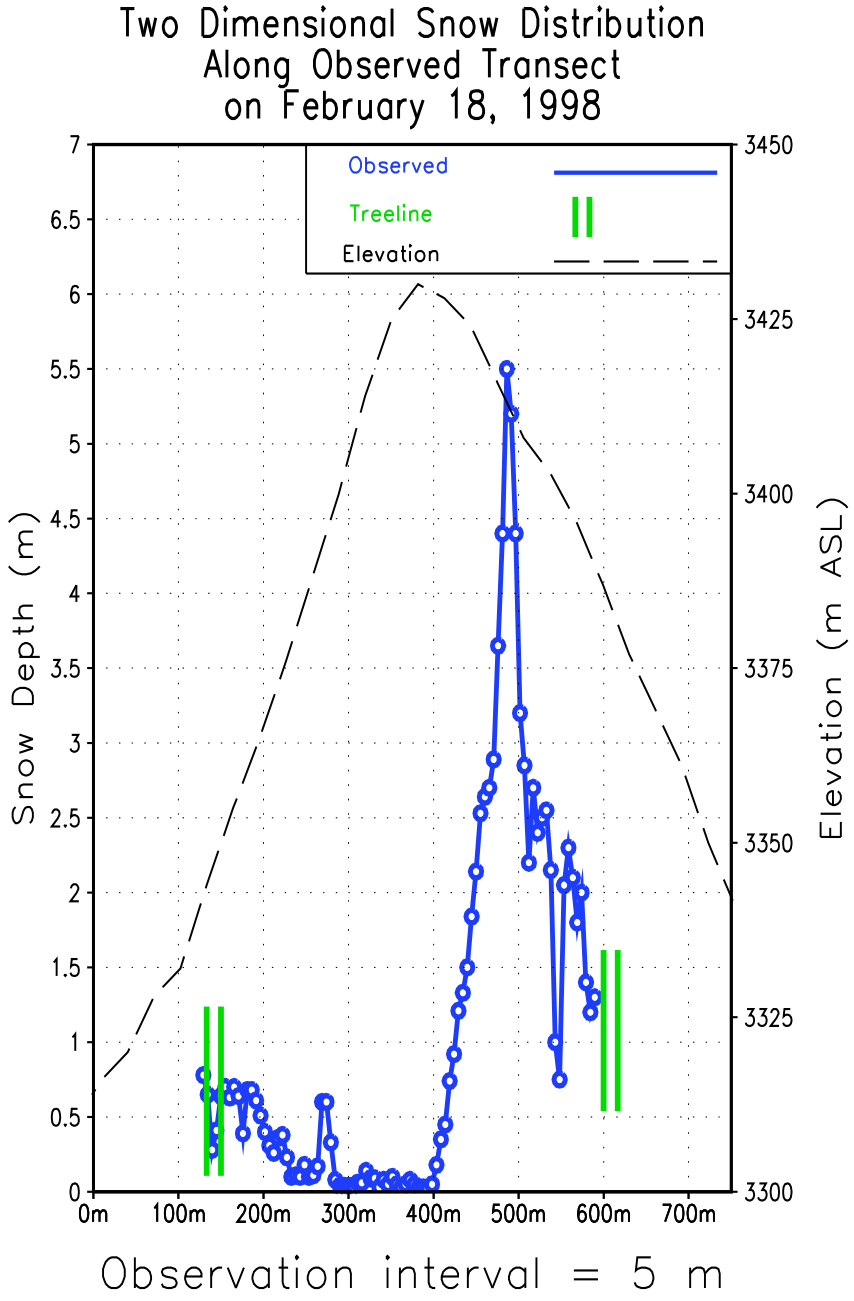

Figure 3.4: Observational transect of snow depth (m) taken on February 18, 1998.

combination of the atmospheric data collected by the instrumentation array, and the adjusted precipitation data from the SNOTEL site were used to drive SnowTran-3D during these simulations.

Since the initial snowdrift distribution was unknown, the model was initialized with the October through December precipitation from the Joe Wright SNOTEL site. The initial precipitation was subject to the same elevation compensation as the daily precipitation. This initial snowcover was assigned a density of 350 kg/m^3; the average density observed from snowpits in the study area. To run SnowTran-3D, several other parameters must be defined, such as the threshold shear stress, the surface roughness length, and the vegetation snow-holding capacity. Values for the parameters used in the simulation are summarized in Table 3.1. In addition, the atmospheric forcing data used to drive the model (air temperature, relative humidity, wind speed, wind direction, and precipitation) are given in Figure 3.5.

Table 3.1: User-defined constants used in model simulations.

C_v		vegetation holding snow-capacity (m)
	5.0	evergreen trees
	0.003	alpine tundra
$z_{0_{\text{veg}}}$		vegetation roughness length (m)
	0.8	evergreen trees (Pielke 1984)
	0.1	alpine tundra
f	500.0	equilibrium fetch distance (m) (Pomeroy et al. 1993)
u_{*t}	0.25	threshold wind shear velocity (m/s) (Schmidt 1986)
$z_{0_{\text{snow}}}$	0.005	snow roughness length (m)
Υ_c	400	topographic curvature weighting factor
Υ_s	10	topographic slope weighting factor
μ	3.0	scaling constant for non-equilibrium saltation transport
ρ_s	350.0	snow density (kg/m^3)
σ_c	0.5	cloud cover faction

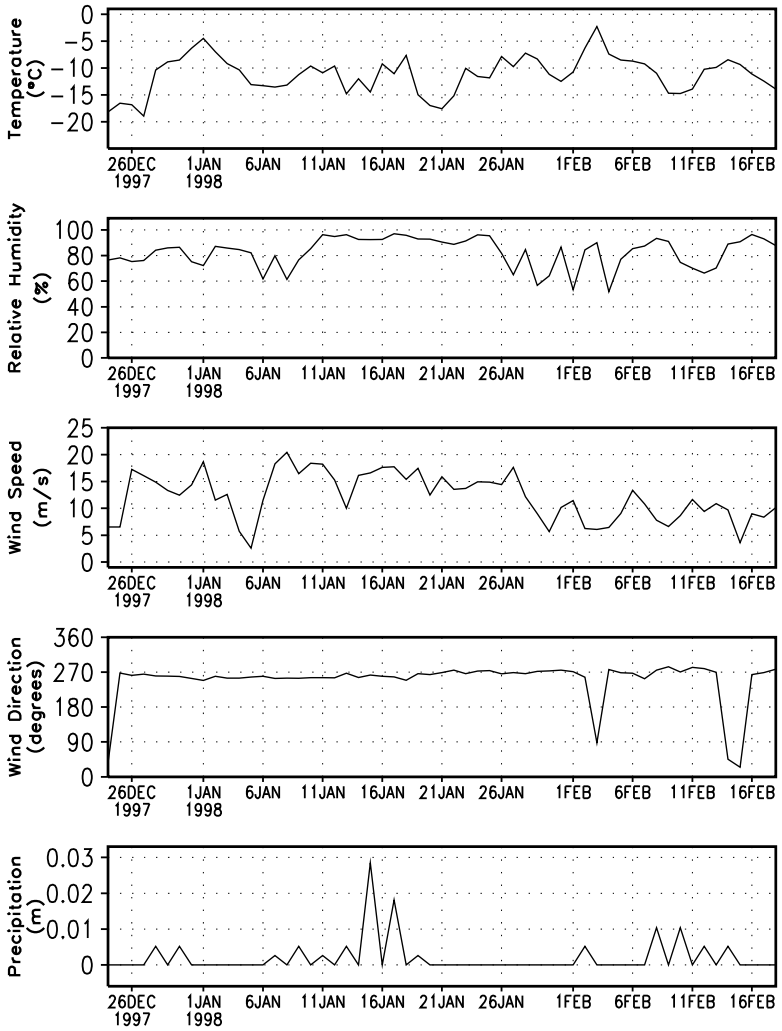

Figure 3.5: December 24, 1997 thru February 18, 1998 daily average observed atmospheric forcing data of air temperature, relative humidity, wind speed, wind direction, and snow-water-equivalent precipitation used in model simulations.

3.5 Results

The model was able to adequately simulate the snow drift distribution across the terrain barrier (Figure 3.6). Persistent westerly winds with velocities greater than 5 m/s (Figure 3.5) eroded the majority of the snow on the west side of the terrain barrier and transported it to the east side. The model left the winter snowpack unaltered within the treed areas, while in the above-treeline areas the snowpack was eroded down to the surface holding capacity (Table 3.1). The general snow-distribution profile and the relationships between treed windward and lee slopes are illustrated in Figure 3.7, where the simulated snow depth has been enhanced by a factor of three in order to make it easier to see the snow distribution. On the east side of the terrain barrier, the model deposited the snow in a well-defined row of drifts that run parallel to and between the ridge-crest and the eastern treeline (Figure 3.8). This snow distribution trend, scoured on the east side with a large drift on the west, was observed to be present along the entire ridgeline (Figure 3.9).

As part of the snow-transport scheme, the model computes the mass of snow returned to the atmosphere due to sublimation of the blowing snow. Dividing this value by the total precipitation input (both initialized and daily precipitation) yields the mass fraction of the snow removed by sublimation. Figure 3.10 shows that over the ridge-crest between 9 and 15% of the snow was returned to the atmosphere by sublimation. Isolated points along the terrain barrier sublimated up to 30% of the period precipitation. These numbers are consistent with the findings of Pomeroy and Gray (1995), and Liston and Sturm (1998) for regions of the Canadian Prairies and North American Arctic.

3.6 Discussion

The model simulation produced a snowdrift profile which compares well with the observed profile. Figure 3.6 shows that the simulated drift has a similar slope and width to the observed drift. The model was also able to simulate the rapid decrease in snow depth at the transition from treeline to alpine tundra on the west side of the terrain barrier (Figures 3.6 and 3.8). The maximum depth of the observed drift is nearly 2 m greater

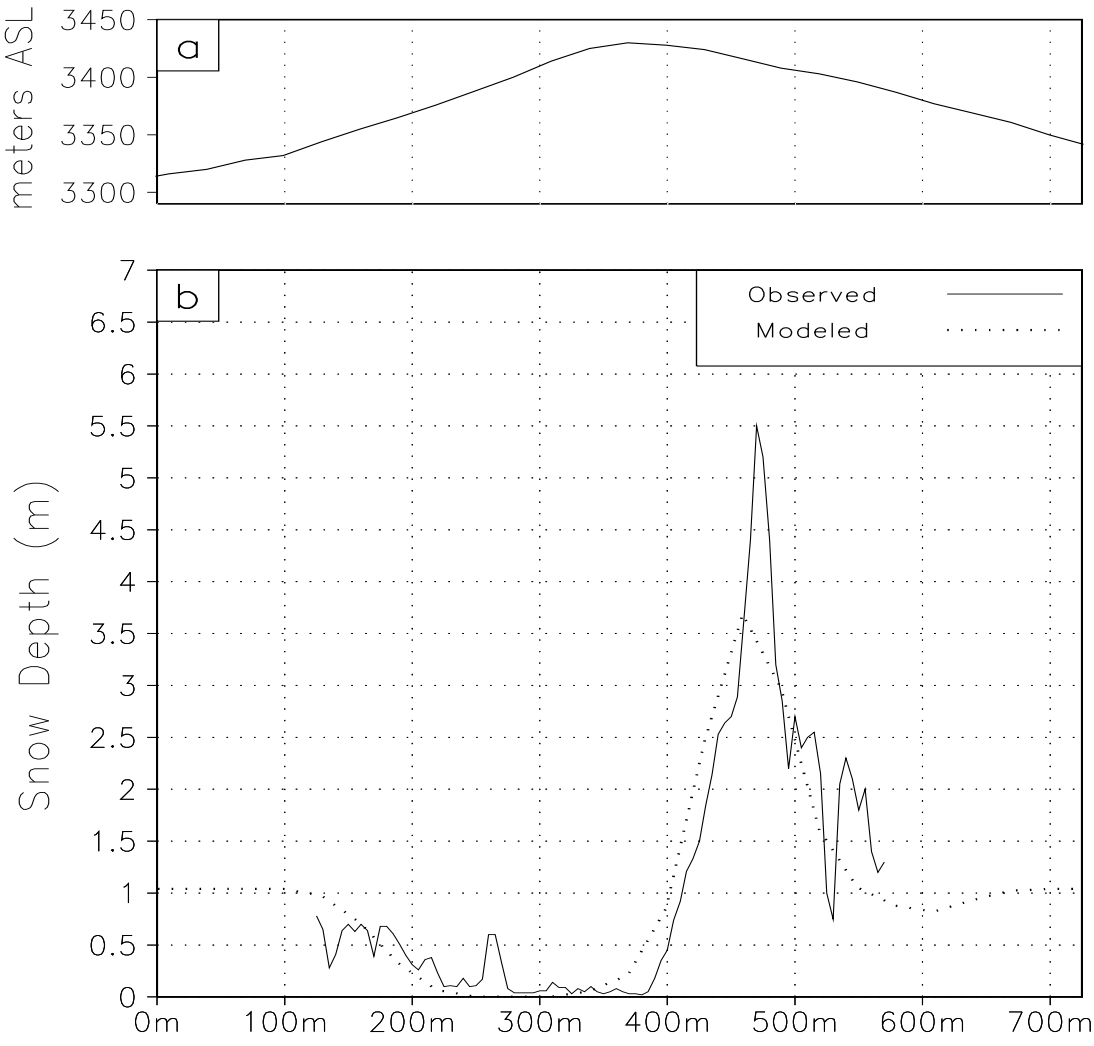

Figure 3.6: a) Cross section of model topography at the location of the observed transect. The ordinate indicates meters above sea level. b) Cross section of modeled and observed snow depths (m) for February 18, 1998.

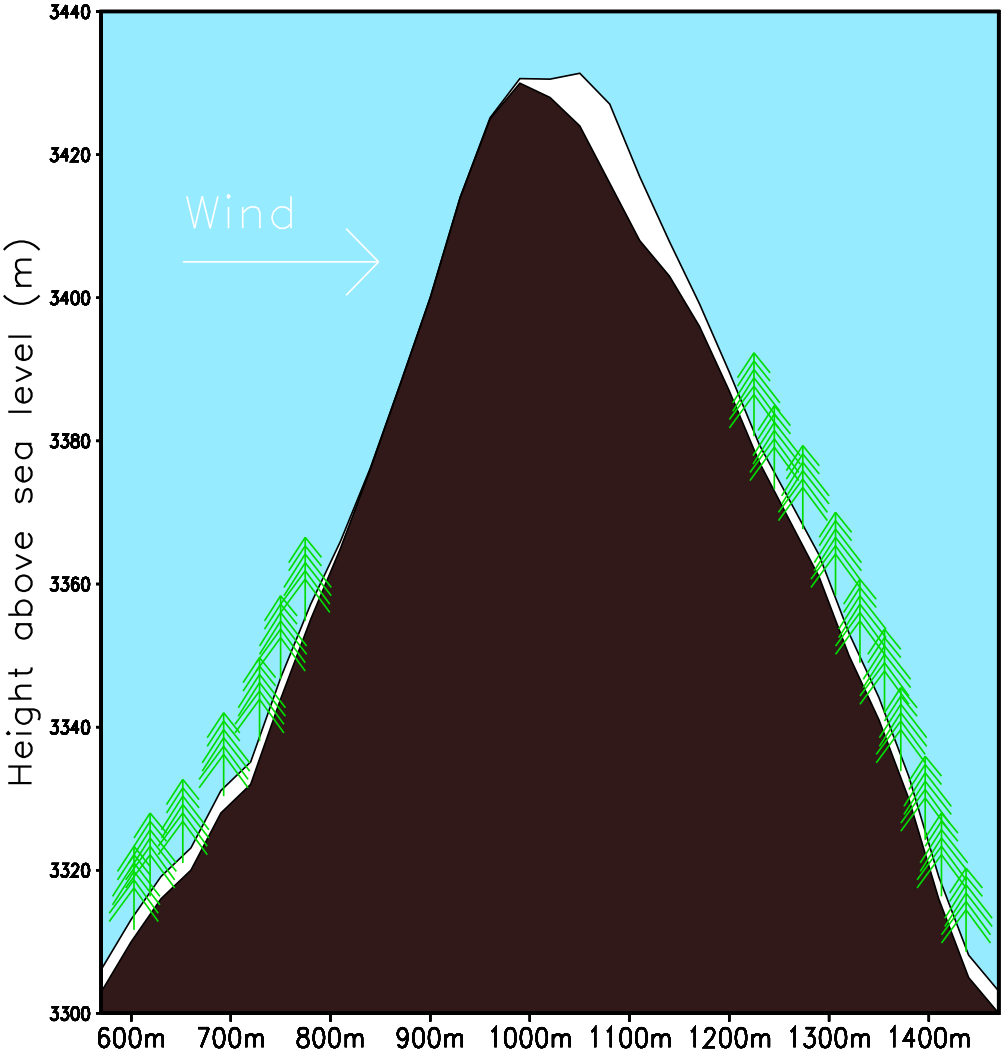

Figure 3.7: Snowdrift profile along observed transect. The snow depth is enhanced by a factor of 3.

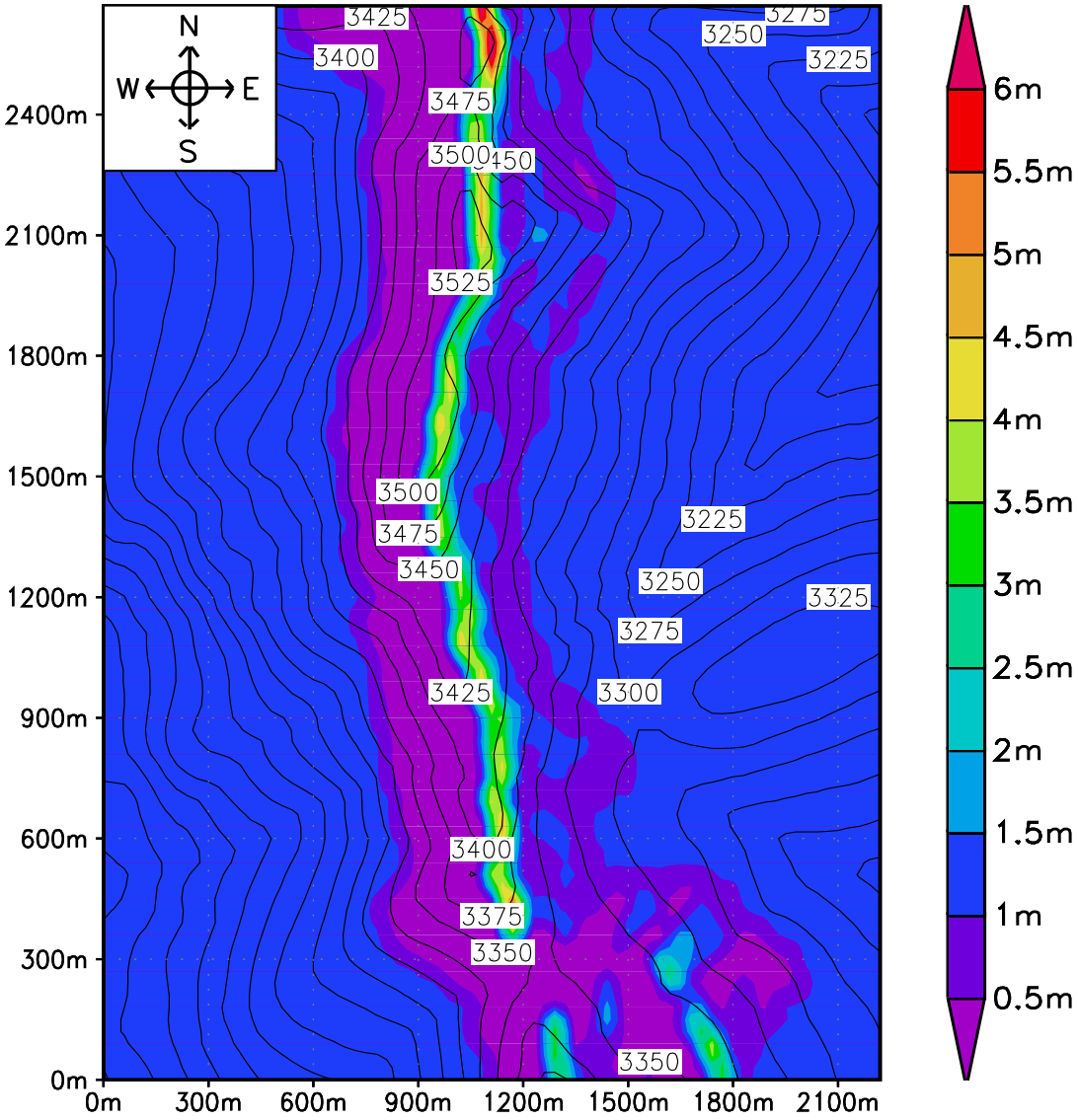

Figure 3.8: Model-simulated spatial distribution of snow depth (m) for February 18, 1998. Contours of topography are in 25 m intervals.

Figure 3.9: Looking south from the Montgomery Pass Weather Station. The snow distribution is similar to that depicted in Figure 3.6 and to that observed along the ridgeline.

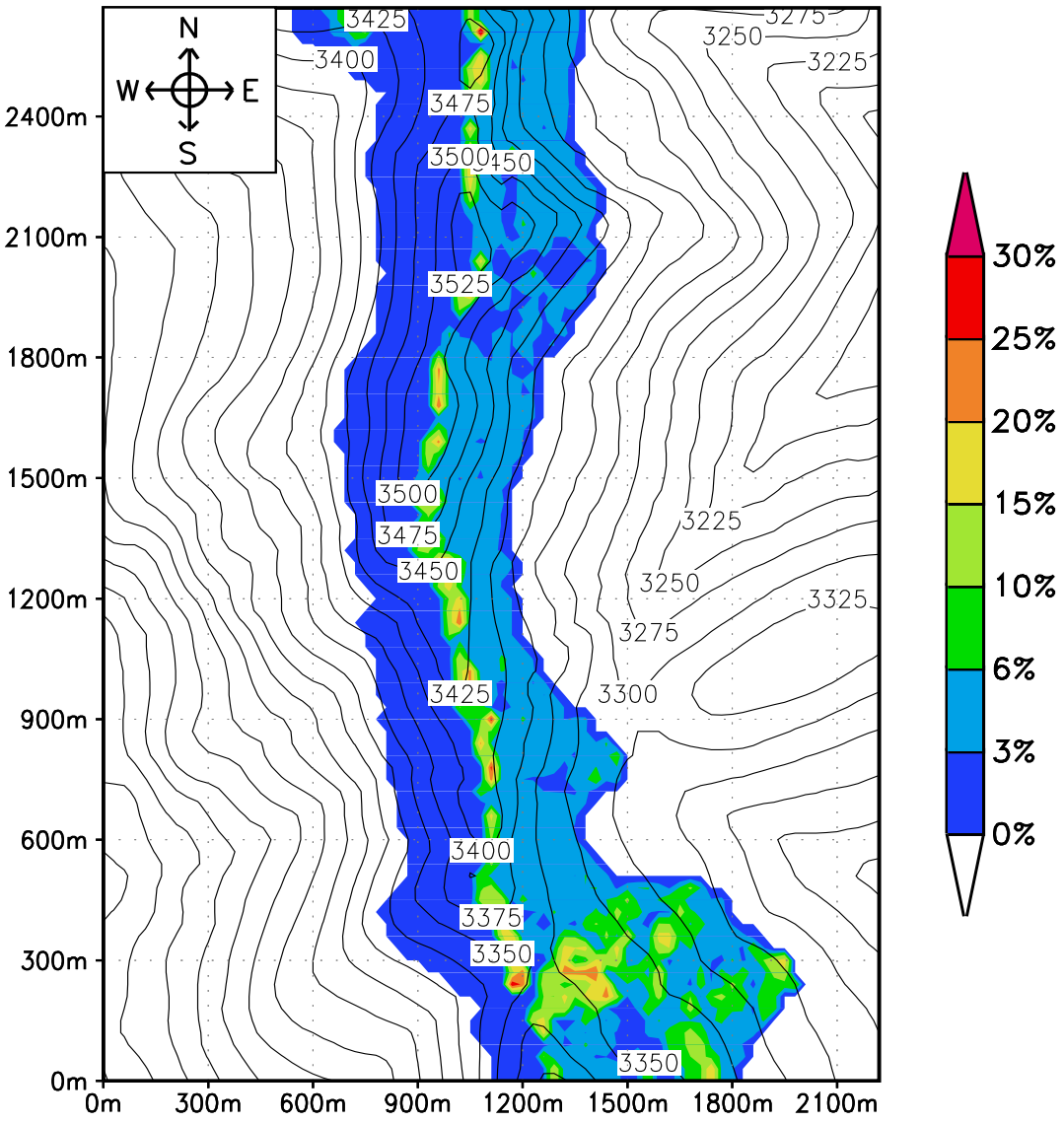

Figure 3.10: Percent of year-to-date (February 18, 1998) snow-water-equivalent removed by sublimation of airborne snow. Contours of topography are in 25 m intervals.

than the simulated drift. We consider this result acceptable due to the difference in grid increment between the observations and the model grid (model $\Delta x = 30$ m, observation $\Delta x = 5$ m). Although the observations show a peak depth of 5.5 m, it is a sharp peak occurring over a distance of 10 m. At the current resolution, the model is unable to resolve features of this scale.

It is difficult to obtain a quantitative value for the amount of sublimation which should occur in this type of environment. The governing physical processes are nonlinear and cannot be directly measured. The model calculates the amount of sublimation using the atmospheric fields provided. However, we have no way of determining the error in these calculations. If our precipitation estimates do not adequately compensate for the elevation differences, the sublimation calculations will be in error.

The least substantiated method used during this study was the precipitation adjustment for elevation differences. Although it is widely accepted that in mountainous regions precipitation varies with location and elevation, a method for adjusting precipitation data that is both reliable and universal has not yet been established. In an alpine area, such as Montgomery Pass, it is difficult to directly measure snowfall accurately due to relatively high winds (Larson 1985).

Due to the combined effects of synoptic weather patterns and topography, the dominant wind direction was from the west. This resulted in the majority of the above-treeline snowpack being eroded from the west side of the ridgeline, and being transported and deposited on the east side. The model simulated the physical processes associated with the wind-transport of snow, building a drift on the east side of the terrain barrier whose location, mass, width, and slope compared well with observations. Given the difference in scales between the model grid and observation interval, the height of the drift also compared well with the observations. An improved precipitation data set, obtained from a position closer to the research site, would have allowed further scrutiny of the model's sublimation calculations.

Chapter 4

SNOWTRAN-3D FORCED BY CLIMRAMS

4.1 Flattop Mountain

4.1.1 Introduction

High elevation weather observations in mountainous regions are scarce. In such areas, where access is often poor, it is impractical to install and maintain weather observing equipment. Hence for the second portion of this study we strived to compute the three-dimensional snow distribution with minimal ground observations. In place of direct observations, output from an atmospheric modeling system was used. The atmospheric forcing fields were produced by the Colorado State University climate version of the Regional Atmospheric Modeling System (ClimRAMS). The atmospheric fields from ClimRAMS were used to drive SnowTran-3D, which in turn simulated the snowcover distribution over the Flattop Mountain plateau. The goal of this portion of the study is to simulate the snow-transport processes that occur on the plateau, and reproduce the observed snow distribution.

The domain of the ClimRAMS and SnowTran-3D simulations was large enough to encompass both the Flattop Mountain and Montgomery Pass sites. Due to the lack of high elevation wind data within Rocky Mountain National Park (RMNP) and the larger area within the Flattop Mountain site, this portion of the study focused on the Flattop Mountain site. Within this chapter, we will first discus the procedures and results as they relate to the Flattop Mountain site. In the second section of this chapter the results at Montgomery Pass will be discussed.

4.1.2 Site Description

Flattop Mountain is located in Rocky Mountain National Park (RMNP). It is part of a north/south oriented plateau that lies on the Continental Divide. The landscape is classified as alpine, and is characterized by a mosaic of short grass, talus, and boulders. The elevation of Flattop Mountain is 3757 m, and the majority of the plateau lies within 100 m of the summit. The position of Flattop Mountain and its relation to Montgomery Pass are shown in Figure 4.1.

4.1.3 Experimental Design

The experimental design for this portion of the study follows a methodology similar to Chapter 3. There was a field component that collected atmospheric and snow distribution data. The data obtained during the field portion were used to guide the modeling portion of the study. However, in this section the atmospheric forcing fields required by SnowTran-3D were produced by another modeling system, ClimRAMS.

Field Observations

In late November 1997, a series of Hobo temperature sensors were installed along a transect from Bear Lake to Grand Lake. The purpose of this portion of the field campaign was to obtain air temperature data within the ClimRAMS simulation domain which could be used to check the atmospheric fields generated by ClimRAMS. The Hobo sensors and data loggers were installed on existing objects such as trees and sign posts. Each temperature sensor was placed in a white plastic cup, and the cup was mounted with the opening facing down (Figure 4.2). This cup served as a radiation and precipitation shield. These sensors sampled the instantaneous air temperature every 144 minutes (the observation increment was dictated by the configuration of the data logger) from late November 1997 until early May 1998.

During the period of February 14-16, Dr. Liston and myself camped at treeline on the east side of Flattop Mountain. During these three days we walked six transects along the Flattop plateau (Figure 4.3). Along each transect the snow depth was measured at 50 m intervals using probe poles marked in 10 cm increments.

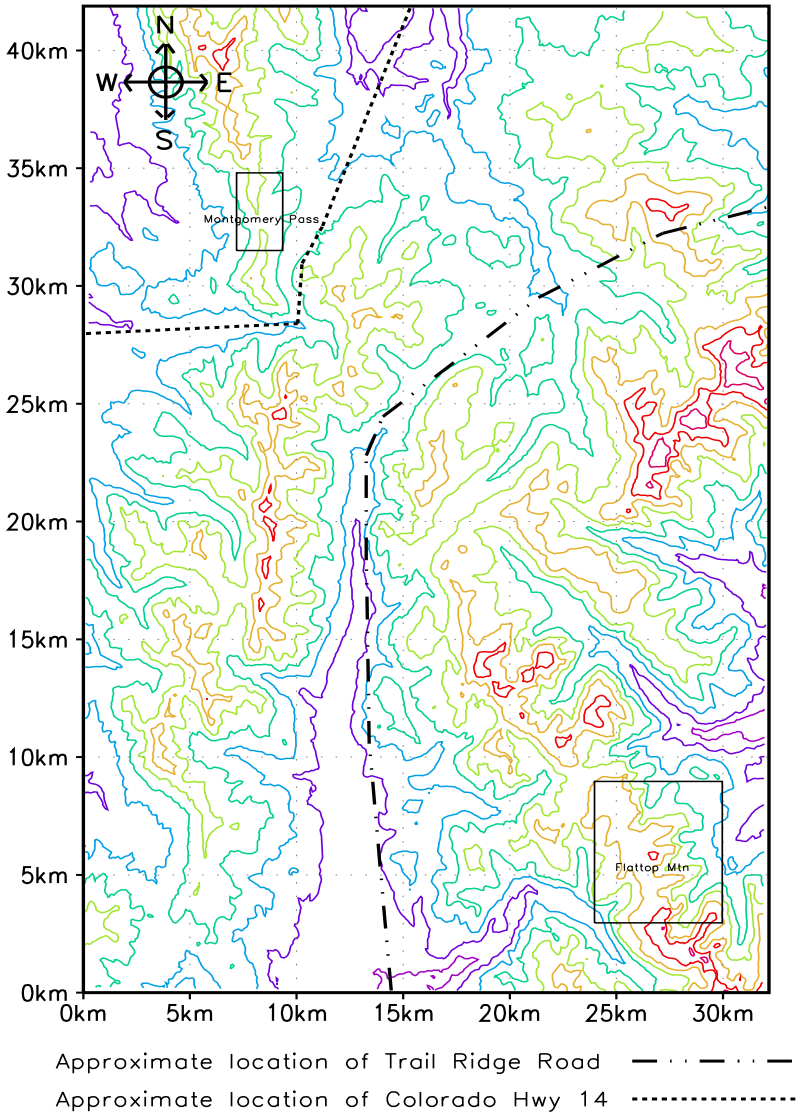

Figure 4.1: Location of Flattop Mountain Site in relation to Montgomery Pass Site. The approximate location of Trail Ridge Road and Colorado Highway 14 are also shown.

Figure 4.2: Field setup of Hobo data logger and air temperature sensor. The temperature sensor is placed in an inverted plastic cup that serves as a radiation and precipitation shield. The data logger is located in a plastic jar below the radiation shield.

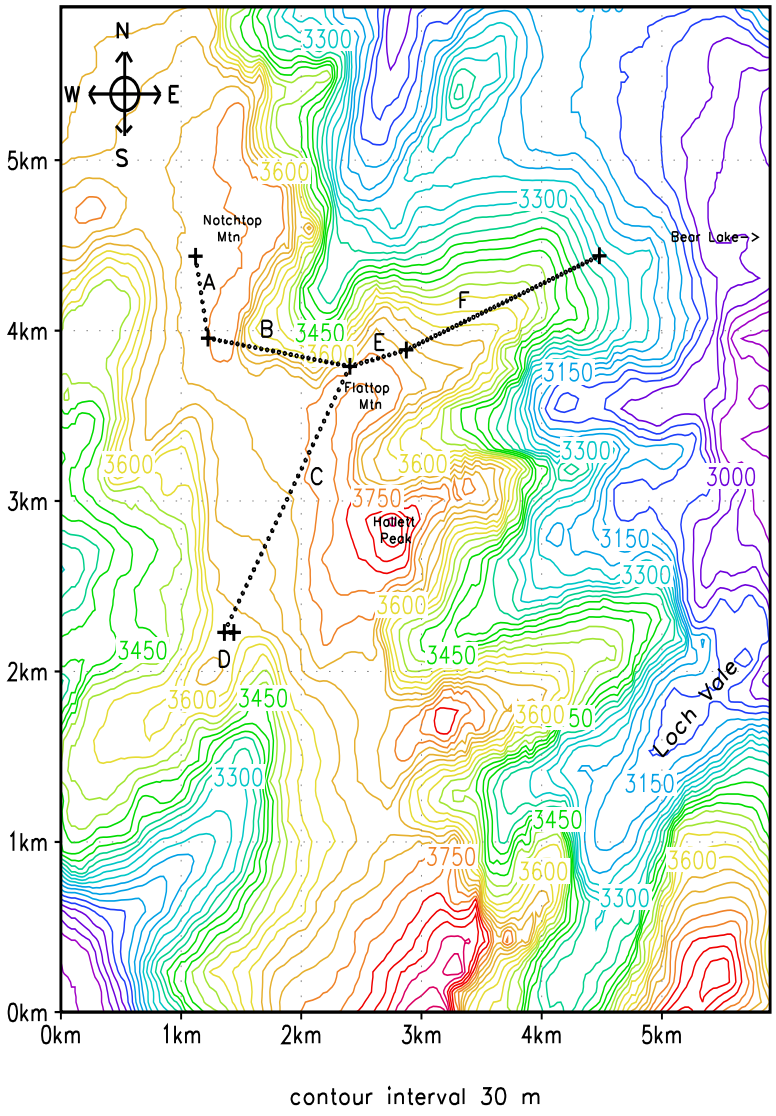

Figure 4.3: Model topography and location of observational transects. Snow depth in meters was recorded in 50 meter intervals along each transect. These transects were conducted between February 14 and 16, 1998. Contours of topography are in 30 m intervals.

In order to compare the observations (50 m spacing) with SnowTran-3D simulations ($\Delta x = \Delta y = 30$ m), the observations needed to be interpolated to the SnowTran-3D grid. This process was completed using a kriging scheme (Deutsch and Journel, 1998). Kriging involves combining a collection of generalized, linearized regression techniques in order to minimize an estimation variance defined from a prior covariance model. The kriged observations are shown in Figure 4.4. A more detailed explanation of the mathematical development of kriging is given in Appendix A.

Model Configuration

ClimRAMS

For this study, ClimRAMS was used to simulate the evolution of the atmosphere from October 1, 1997, through March 31, 1998, a period of 182 days. For these simulations the model used three nested grids. Grid 1 extended from just off the west coast of the United States into the central Great Plains at a horizontal grid spacing of 100 km ($\Delta x = \Delta y = 100$ km) (Figure 4.5). Grid 2 is nested within Grid 1 and covers northern Colorado and Southern Wyoming at a horizontal grid spacing of 25 km ($\Delta x = \Delta y = 25$ km). Grid 3 covers the mountains of Northern Colorado including Rocky Mountain National Park and Montgomery Pass at a horizontal grid spacing of 5 km ($\Delta x = \Delta y = 5$ km). The model contains 20 vertical levels. The spacing of the vertical levels was 0.125 km at the lowest level and increases with increasing altitude, but never exceeds 2 km. Model integrations for grid one, two, and three were performed using a time step of 120 s, 60 s, and 15 s respectively.

The model used the present-day vegetation distribution, and the standard RAMS methodology to define the vegetation type, areal fraction and leaf area index (Liston et al. 1999). The vegetation-classification data were obtained from the Earth Resources Observation Systems (EROS) Data Center Distributed Archive Center (EDC DAAC), located at the United States Geological Survey's (USGS) EROS Data Center in Sioux Falls, South Dakota (http://edcwww.cr.usgs.gov/landdaac/). The model topography is defined using a global, 30 arc-second latitude-longitude topographic data set called GTOPO30

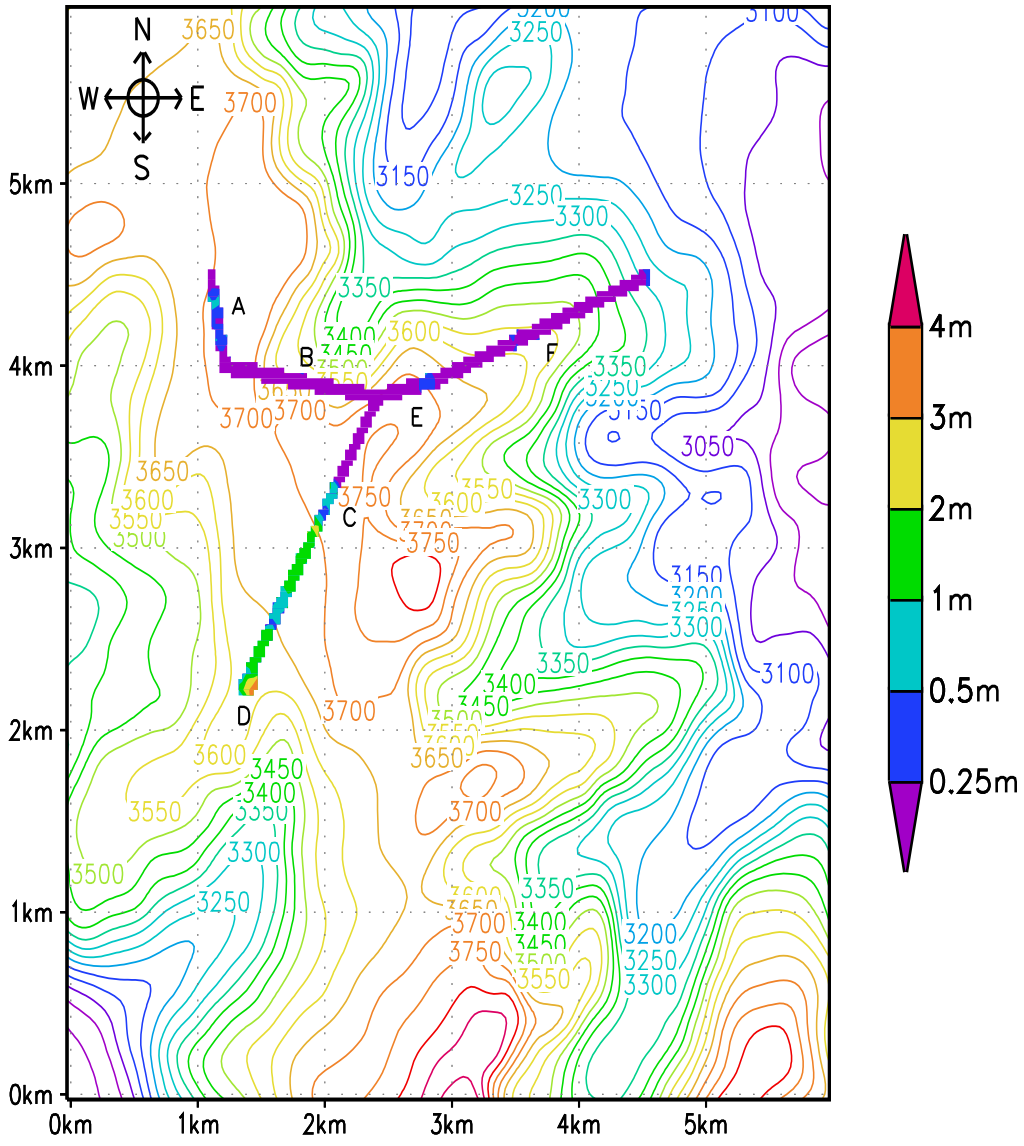

Figure 4.4: Snow depth observation after kriging has been performed. Contours are of topography in 50 m intervals.

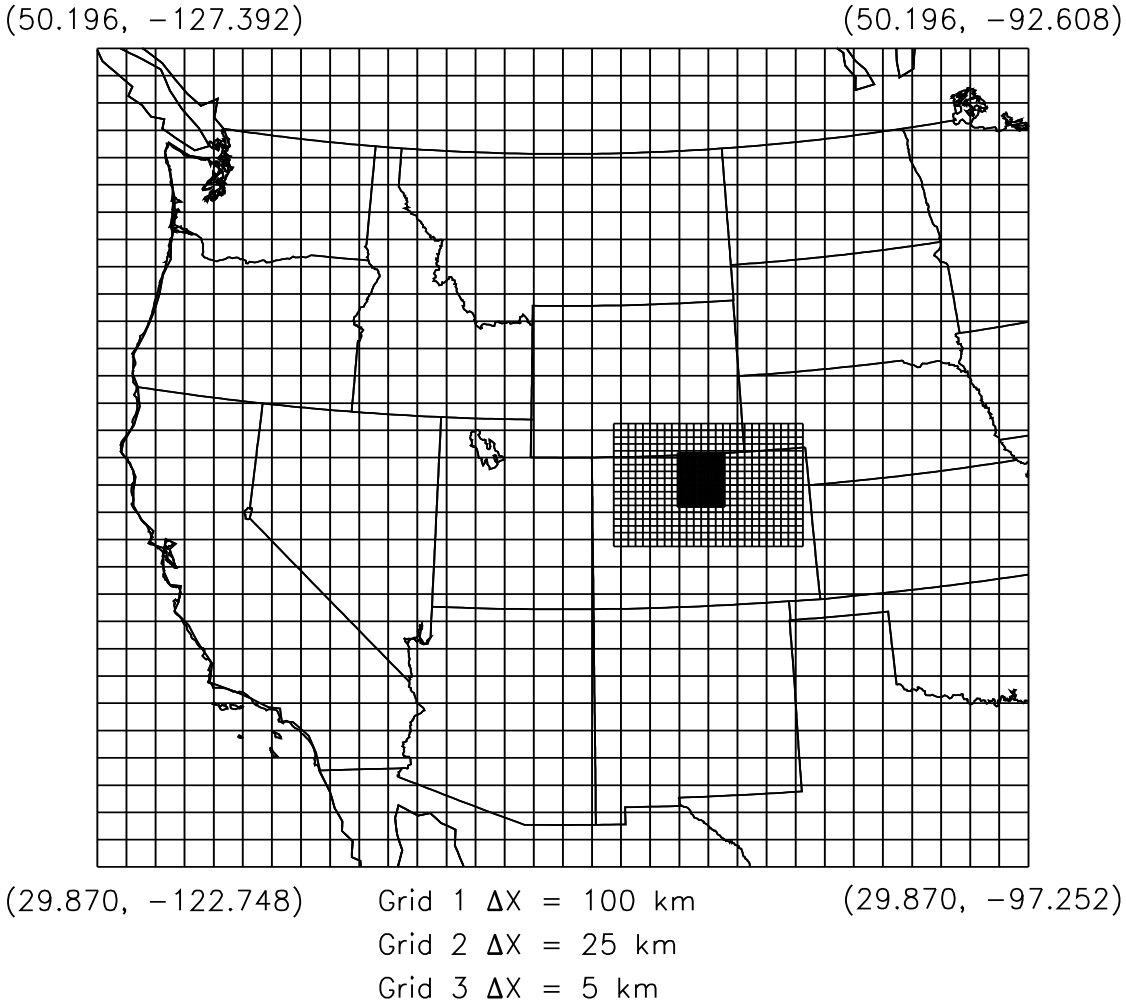

Figure 4.5: ClimRAMS simulation domain and grid configuration. The corner coordinates of grid one in degrees latitude and longitude appear in parentheses.

(Gesch et al. 1999). These data are also available through the USGS EROS Data Center. In processing these data for the ClimRAMS grids, procedures were implemented to ensure compatibility of terrain heights between nested model grids, while allowing higher-resolution terrain features to be included in the finer grids.

For the simulations utilized during this study, the "dump-bucket" precipitation scheme was used. This method is the simplest and most computationally-efficient precipitation parameterization available in ClimRAMS. The scheme is based on an orographic precipitation model (Rhea 1978) and is currently used in the RAMS forecast model (Cotton et al. 1995). In this parameterization, water vapor in excess of saturation is assumed to condense. The precipitation amount is then computed and removed from the saturated layer by applying a precipitation efficiency that is a function of the saturated-layer temperature. The resulting precipitation is assumed to reach the ground without further interaction within the atmosphere. This method does not distinguish between the various types of precipitation (e.g., rain, snow, hail), and thus additional information is required to identify whether liquid or ice-phase precipitation reaches the ground. This delineation is achieved by assuming that when the air temperature in the lowest atmospheric model layer is less than 2.0°C, snow reaches the ground; all other conditions lead to rain (Auer 1974).

ClimRAMS uses global, six hourly, reanalysis data sets from the National Centers for Environmental Prediction (NCEP) (Kalnay et al. 1996) to define the initial and lateral boundary conditions. The reanalysis data are available on a 2.5° latitude by 2.5° longitude vertical pressure-level grid. These data were interpolated to Grid 1 and used to update the lateral boundary conditions of this coarsest grid every 6 hours. This technique forces the large-scale atmospheric patterns in the model to be consistent with observed patterns, while allowing the model to adjust to surface changes within the domain and alter small-scale processes.

SnowTran-3D

The domain for the SnowTran-3D simulations covered an area comparable to the smallest ClimRAMS grid. The simulation domain encompasses most of Rocky Mountain

National Park, and extends north past Montgomery Pass and Clark Peak (Figure 4.1). SnowTran-3D was run over a 1300 km^2 area, with a grid spacing of 30 m ($\Delta x = \Delta y = 30$ m), and used a daily time step, starting October 1, 1997 and ending March 31, 1998.

The topography used in SnowTran-3D was defined using a 30 m digital elevation model (DEM) from the United States Geological Survey. These data depict similar detail to a 7.5 minute quadrangle, and cover an area equivalent to six, 7.5 minute quadrangles.

The model also requires vegetation data which corresponds to the DEM. A 30 m vegetation data set for RMNP was provided by Jill Baron and Melannie Hartmann of the Natural Resources Ecology Laboratory, Colorado State University. This data set was modified so that it contained only five vegetation classifications (trees, grass, shrubs, rocks, water). Although rocks and water are not vegetation, they are part of the landscape and were therefore included in the vegetation data set. For the areas within the simulation domain but outside of RMNP, vegetation type was assigned according to elevation. Areas below 3333 m in elevation were classified as trees. Areas with elevations between 3334 m and 3545 m were classified as grass, and areas above 3546 m were classified as rocks. These thresholds were determined from observations and the vegetation classification on USGS maps. For many applications this type of methodology would not be appropriate. However in SnowTran-3D, the vegetation classification is primarily used to define the snow holding capacity of the vegetation, and since a more detailed vegetation data set does not exist, this method was assumed adequate. The vegetation snow-holding capacity, along with other user defined parameters for SnowTran-3D, are displayed in Table 4.1.

The atmospheric forcing required by SnowTran-3D came from the ClimRAMS simulations. Due to the discrepancy between the grid sizes ($\Delta x = \Delta y = 5$ km for ClimRAMS grid 3, $\Delta x = \Delta y = 30$ m for SnowTran-3D), the ClimRAMS data needed to be interpolated to the SnowTran-3D grid. This process was accomplished using a bilinear interpolator. This post-processing produced spatially and temporally evolving fields of air temperature, relative humidity, wind speed, wind direction, and precipitation on the SnowTran-3D grid.

In order to produce a snow distribution which resembled the distribution observed, we used the limited atmospheric observations we had to guide the modeling portion of this

Table 4.1: User-defined constants used in model simulations that differ from those defined in Table 3.1.

C_v	vegetation holding-snow capacity (m)
5.0	trees
0.5	shrubs
0.4	grass
0.4	rock
0.001	water/ice
$z_{0_{\text{veg}}}$	vegetation roughness length (m) (Pielke 1984)
0.80	trees
0.1	shrubs
0.03	grass
0.01	rock
0.01	water/ice

study. A consistent methodology was followed. The modeled field and the observation were compared for each atmospheric field that had a corresponding observation. If a systematic error was detected, a correction was applied to that field.

One technique for determining model skill is to compute the standard deviations of the modeled and observed data and the root mean squared error (Keyser and Athens 1977; Pielke 1984). In general skill is demonstrated when:

$$\begin{array}{lrcl} (a) & \sigma & = & \sigma_{\text{obs}} \\ (b) & E & < & \sigma_{\text{obs}} \\ (c) & E_{UB} & < & \sigma_{\text{obs}} \end{array}$$

Where $\sigma, \sigma_{\text{obs}}, E$, and E_{UB} are the standard deviations of the modeled and the observed field, the root mean squared error, and the unbiased root mean squared error, respectively. The air temperature data from the Flattop Mountain summit Hobo sensor and the corresponding grid cell from the ClimRAMS grid were compared using this technique. The particular values are:

$$\begin{aligned} \sigma &= 5.27^{\circ}\text{C} \\ \sigma_{\text{obs}} &= 4.26^{\circ}\text{C} \\ E &= 15.67^{\circ}\text{C} \\ E_{UB} &= 2.53^{\circ}\text{C} \end{aligned}$$

Since the values of σ and σ_{obs} are very similar (they differ by one), for our purposes criterion a is satisfied. Criterion c is also satisfied, hence the model demonstrated skill satisfying two of the above three criterion. However this analysis does indicate the presence of a model bias.

As a further comparison, the modeled and observed air temperatures were plotted on the same figure. Although the observed temperatures and the model data are on different time scales (sample time for the observations is approximately 144 min, and for ClimRAMS is 1 day) it is evident from this comparison (Figure 4.6) that ClimRAMS is capturing the large-scale weather features (synoptic signal). However, ClimRAMS consistently produces colder temperatures than those observed. On average, over the simulation period, this difference was 11°C. This correction was applied to the modeled air temperature data used to drive SnowTran-3D.

There were no above treeline wind data available from within RMNP during winter 1997-1998. However, the ClimRAMS simulation domain extended north encompassing Montgomery Pass. The wind speed data from the Montgomery Pass weather station were compared with the ClimRAMS grid cell located over Montgomery Pass. Again this comparison showed that the model was able to capture the synoptic signal, but produced wind speeds of lesser magnitudes than those observed (Figure 4.7). Over the simulation period, ClimRAMS on average underestimated the wind speed by a factor of 2.8. Hence this correction was applied to the wind speed field used in SnowTran-3D.

Many studies have shown that precipitation amounts vary with location and elevation in mountainous terrain (Hjermstad 1970; Baopu 1995; Johnson and Hanso 1995; Snook and Pielke 1995; Obleitner and Mayr 1996). Unfortunately there are no precipitation observations near Flattop Mountain. The closest precipitation observation is a SNOTEL site at Bear Lake. This site lies 7 km to the east and 850 m below the Flattop Mountain summit. The total recorded precipitation (October 1 thru February 15) from the snow pillow at the Bear Lake SNOTEL site was compared to the corresponding ClimRAMS grid cell. This comparison showed that ClimRAMS underestimated the precipitation by a factor of 3. This correction was applied to the precipitation field used in SnowTran-3D. It

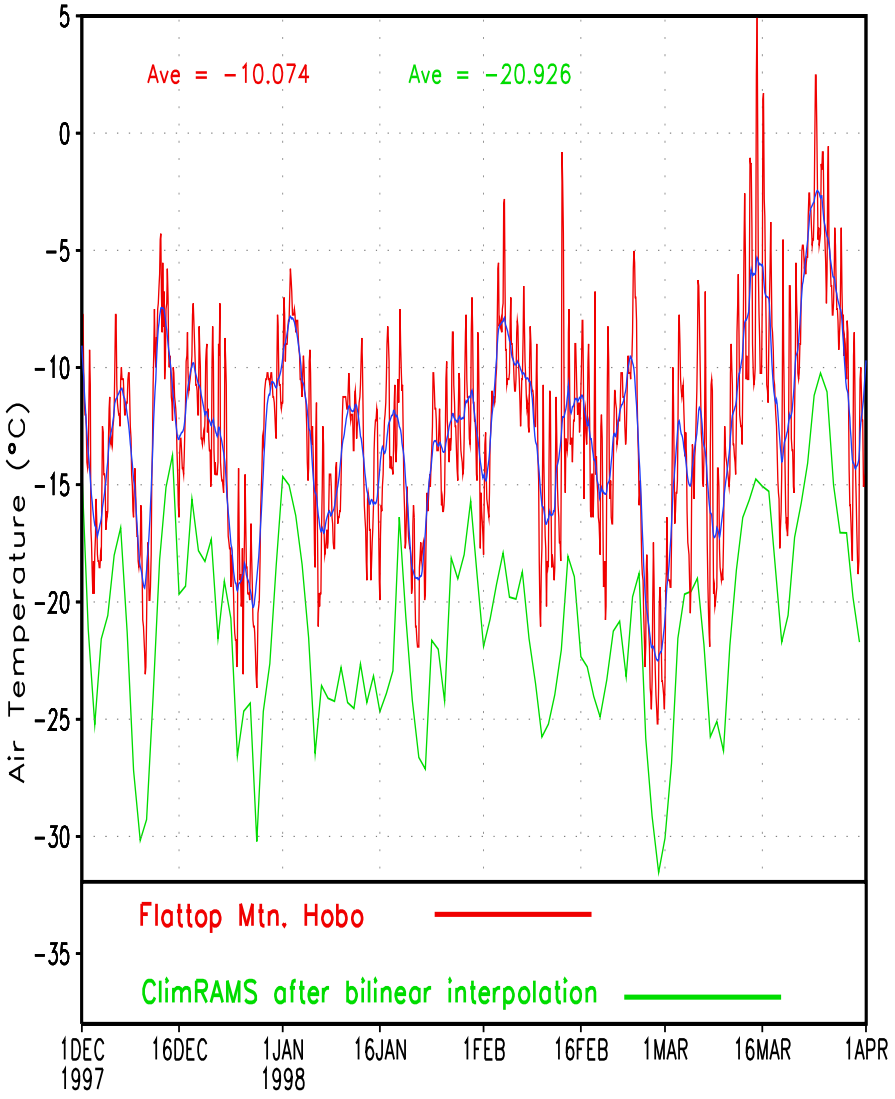

Figure 4.6: Comparison of observed and modeled air temperature. The observations are from the Flattop Summit Hobo temperature sensor. The blue line is approximately a daily average of the observed temperature data. The modeled field is from the ClimRAMS simulation.

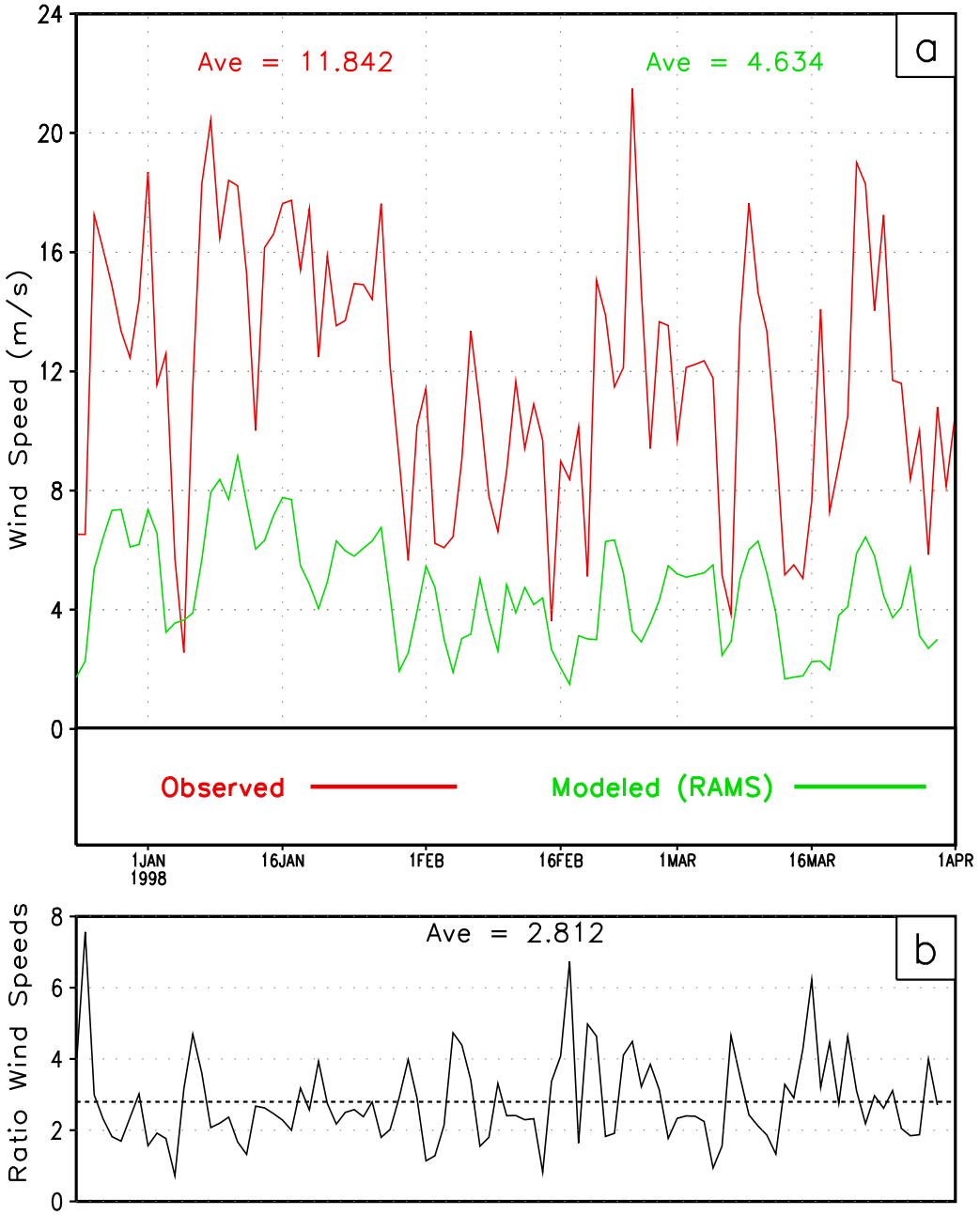

Figure 4.7: a) Comparison of observed and modeled wind speed. The observations are from the Montgomery Pass Weather Station, and the modeled field is from the ClimRAMS simulation. b) Wind speed observations from the Montgomery Pass weather station divided by the screen height wind speed from ClimRAMS.

is well known that dramatic precipitation gradients occur in mountainous terrain. Using this technique in no way ensures that the correct amount of precipitation is used in the model; however, it can be used to estimate the lower limit of that field.

4.1.4 Results

Flattop Mountain and the adjacent plateau are alpine areas characterized by low lying vegetation and rocks. At an elevation of 3757 m, it can be a truly windy place. While conducting field work at this site, it was common to observe wind velocities of 20 m/s. The atmospheric fields produced by ClimRAMS for above treeline areas (Figure 4.8), and adjusted as described in the previous discussion, show the average wind speed during the simulation period to be nearly 15 m/s. The threshold wind velocity for snow transport is generally considered to be 5 m/s (Schmidt 1980; McClung and Schaerer 1993; Li and Pomeroy 1997). Hence, in this region, when snow is available for transport there are strong enough winds to initiate and facilitate snow transport. By examining the wind direction only when the wind speed is equal to or greater than 5 m/s, the average direction of transport was determined (Figure 4.9). For the above treeline areas of RMNP, the average direction of transport is 238°WSW (Figure 4.8). This pattern of persistent westerly winds with magnitudes greater than the threshold for transport is the first-order process affecting snow distribution on the plateau.

In mountainous areas where the wind velocities are typically high enough to transport snow, and the wind direction is generally consistent, we would expect to see a scoured windward side of the mountain range and snow drifting occurring on the leeward side. This pattern was both observed and simulated during the course of this study. Figure 4.10 depicts the simulated three-dimensional snow distribution on February 15, 1998 (the date on which the observations were taken). The simulated snow distribution shows that the model was able to capture the dominant snow transport processes, scouring the plateau and building deep drifts in the east facing cirques.

Over the western portion of the domain, where the vegetation snow-holding capacity is shallow enough to be exceeded by the period precipitation, snow transport occurs. In these areas the wind erodes the snow until only that which is captured by rocks and

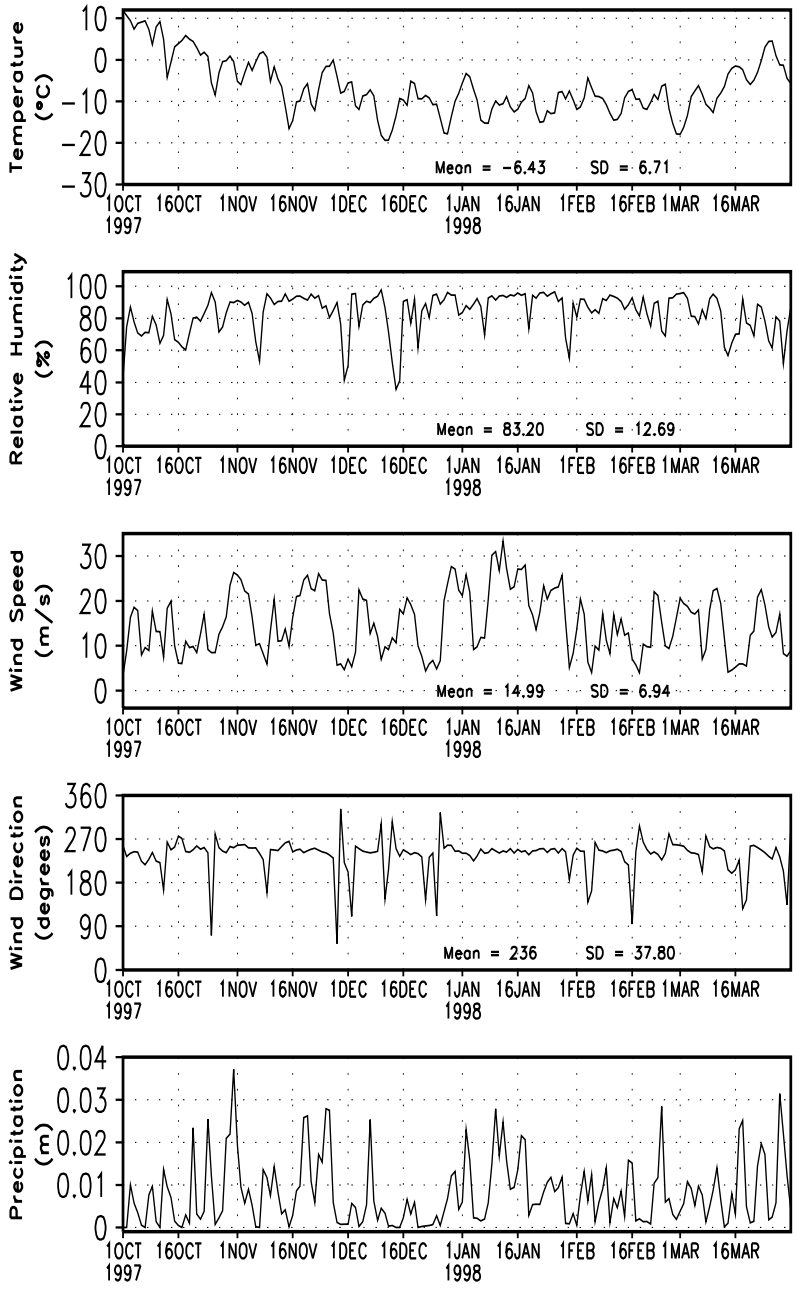

Figure 4.8: Atmospheric forcing data produced by ClimRAMS and used by SnowTran-3D. The values shown are averaged over the above treeline areas of the SnowTran-3D domain. In these plots the air temperature, wind speed, and precipitation values have been adjusted as discussed in the text.

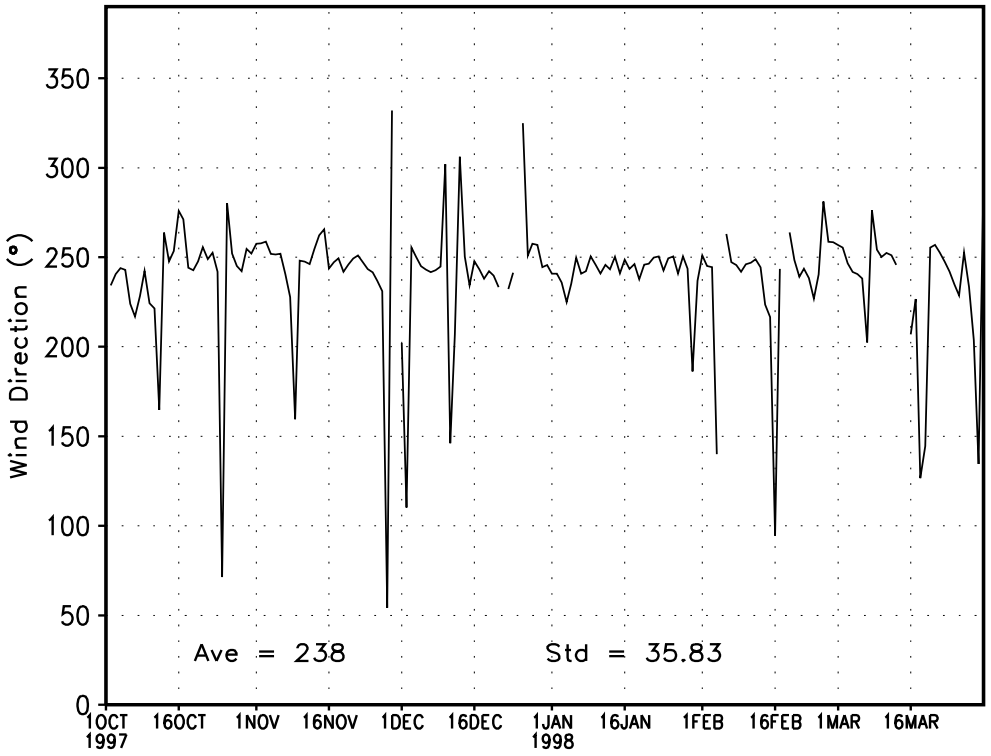

Figure 4.9: Wind direction during blowing snow events. Blowing snow events are defined as events where the wind speed is greater than 5 m/s.

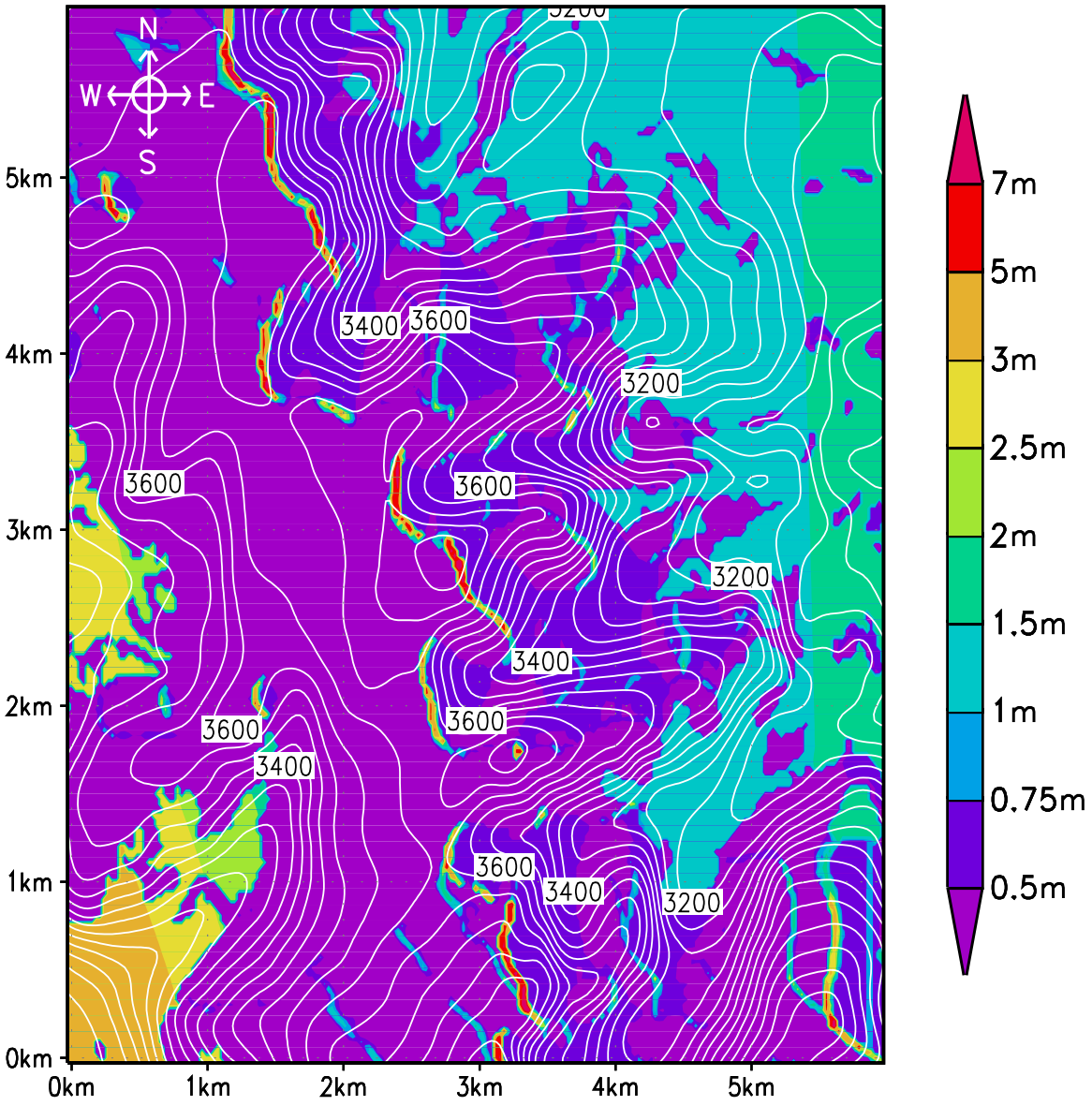

Figure 4.10: Simulated three-dimensional snow distribution produced by SnowTran-3D for the Flattop Mountain Site on February 15, 1998. Contours of topography are in 50 m intervals.

vegetation remains. Throughout the entire domain in areas where the vegetation snow-holding capacity is not exceeded by the period precipitation, all of the precipitation input to SnowTran-3D remains. Thus precipitation gradients produced by the 5 km ClimRAMS grid can be seen in the forested areas of the domain. This gradient appears in Figure 4.10 as bands parallel to the ridgeline on either side of the Continental Divide. Along the plateau where small catchment areas exist, snow drifts were formed. However, for the most part, the snow was transported to the east side of the plateau and either sublimated along the way or deposited into drifts on the leeward side of the plateau.

To evaluate the model's performance on the Flattop Plateau, the ratios of the observed snow depths to the simulated snow depths were calculated. As previously stated, the snow depth observations were taken along two-dimensional transects on February 15, 1998. The ratio of the observed to modeled snow depth for this date is displayed in Figure 4.11. The average of this ratio, over all six transects, is 0.975. The average is very close to unity which suggests the model successfully simulated the distribution of snowcover along the plateau. However, closer examination of Figure 4.11 reveals almost equal areas where the ratio (observed/model) is quite small, near unity, and quite large. Hence the model successfully simulated the snowcover distribution over part of the area, but was unable to capture many of the features observed.

As part of the SnowTran-3D mass balance computation for each grid cell, the mass of snow removed due to sublimation of airborne snow is calculated. We can estimate the percent of the annual precipitation input that is returned to the atmosphere due to sublimation by dividing this calculated value by the amount of precipitation which falls in that grid cell. The percent of annual precipitation removed due to sublimation for the Flattop Mountain site is displayed in Figure 4.12. In the majority of the study site, less than 20% of the seasonal snowcover is removed by sublimation of airborne snow. Keep in mind that in forested areas the annual precipitation never exceeds the vegetation holding capacity set in SnowTran-3D. As a result there was never any snow available for transport and thus no sublimation occurred. However in areas where snow was transported, there are large sections where greater than 40% of the seasonal snow was returned to the atmosphere

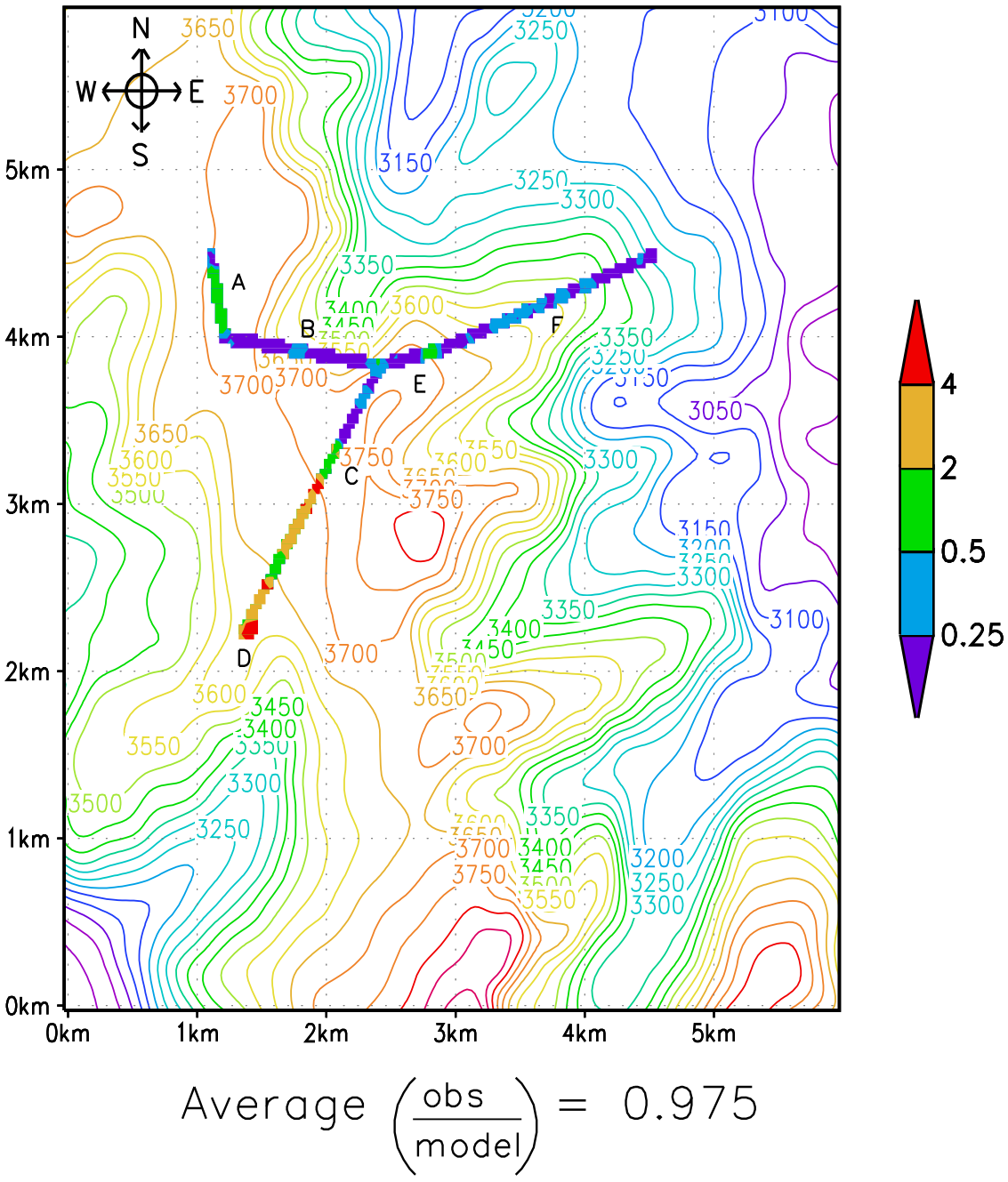

Figure 4.11: Ratio of observed to modeled snow depth along observational transects for February 15, 1998. Contours of topography are in 50 m intervals.

by sublimation. There are also narrow regions along the tops of the east-facing cirques where more than 100% of the seasonal snow was sublimated. Intuitively it does not make sense for more than 100% of the precipitation to be removed due to sublimation. Since snow is continuously being transported into these grid cells, there is a greater mass concentration of airborne snow than would exist from precipitation alone. Hence more snow can sublimate out of these grid cells than has fallen into them from precipitation events.

4.1.5 Discussion

The goal of this portion of this study was to use an atmospheric modeling system to drive a snow-transport model. Merely using one model to drive another would be of little significance if the result were not at least intuitively correct. Our desire was also to simulate the evolution of seasonal snowcover in a alpine setting. On the large scale, this goal was accomplished. The simulated snow distribution generally depicts the observed snow distribution, scouring the snow from the west side of the plateau and depositing it in large drifts on the east side. The model also built large drifts along the tops of the east facing cirques along the plateau. These deep drifts were observed and contribute to the formation of perennial snow fields and glaciers in several of the drainages. As a visual example of the drifts that form in RMNP, Figure 4.13 shows the Tyndall Glacier. Several other of the east facing drainages also contain features similar to the Tyndall Glacier.

The depths of the individual drifts are sensitive to the amount of precipitation and sublimation that occur within the domain. The amount of sublimation that occurs is sensitive to the air temperature, wind speed, and relative humidity of the atmosphere's lowest layer. However, in an area like the Flattop Mountain Plateau where the winds generally are so strong that the snowcover is reduced to the vegetation snow-holding capacity in virtually all areas except the drift traps, the location of the snow drifts and the resulting accumulation patterns are most affected by the wind direction. Hence changes in the atmospheric fields, with the exception of wind direction, would have little effect on the location of the major snow drift features produced by this simulation. Rather, such

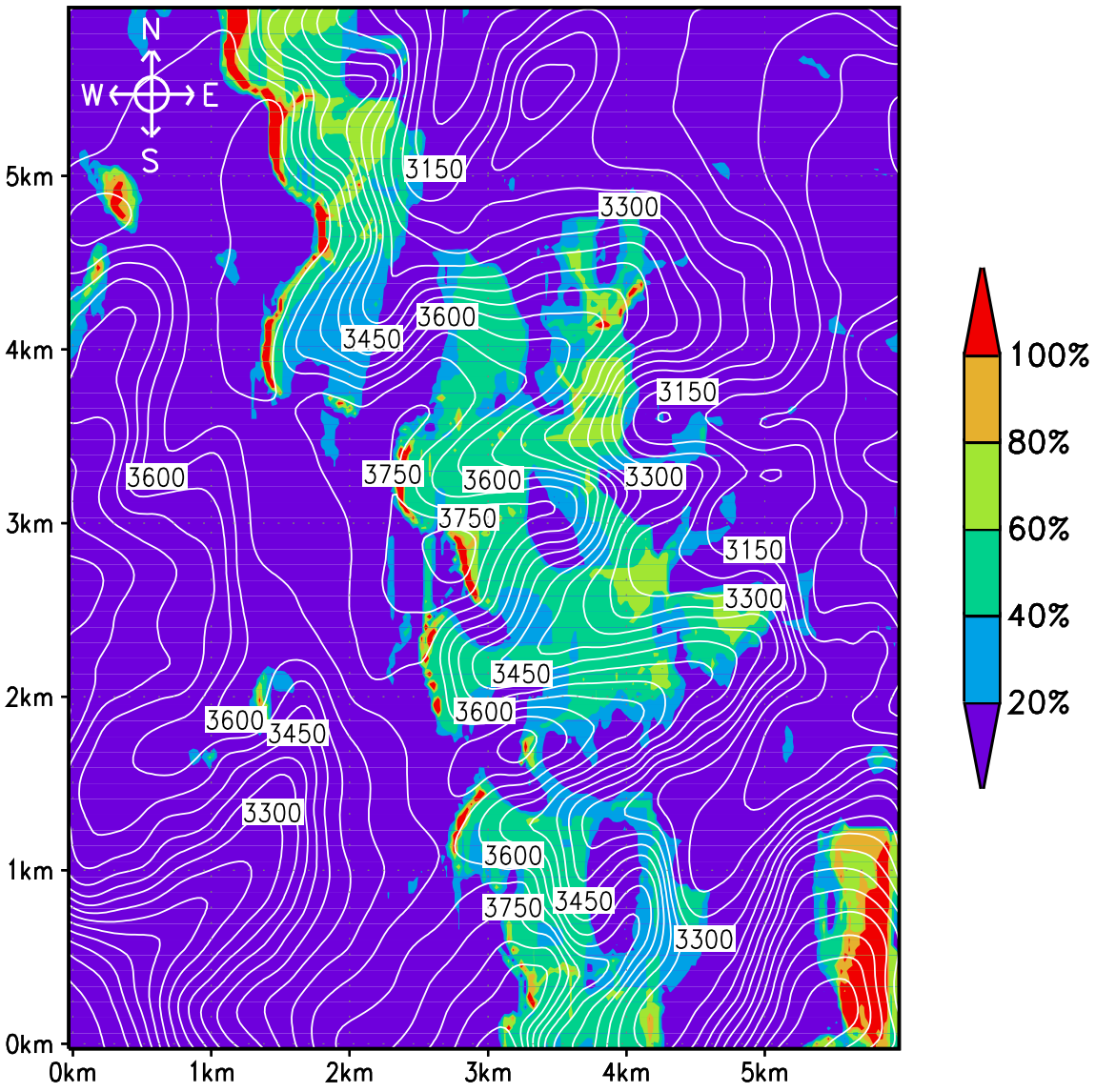

Figure 4.12: Percent of year-to-date precipitation which was removed due to sublimation of airborne snow for the Flattop Mountain Site. This is the distribution for February 15, 1998. Contours of topography are in 50 m intervals.

Figure 4.13: Tyndall Glacier in August, southeast of Flattop Mountain. Several perennial snow fields similar to the Tyndall Glacier occur along the east side of the Continental Divide within Rocky Mountain National Park.

changes would alter the snow depth and horizontal extent of these snow accumulation features.

There were many small-scale drifts which the model was unable to simulate. These drifts are the result of two factors. First, on the plateau there exists gently rolling topography. Many of these rolls are large enough that snow drifts form around them. However, their horizontal extent is small enough that they are not resolved by the 30 m DEM used by SnowTran-3D. As a result, SnowTran-3D does not produce snow drifts in some of the areas where they are observed. The presence of such drifts, and the inability of the model to simulate them can be seen along the C transect in Figures 4.4 and 4.11, respectively. Second, many drifts occurred in the lee of small to large boulders. These features are large enough to create snow drifting but are not resolved in the topographic data set.

Although there was careful consideration of site location, the Flattop plateau may not have been the best site for this study. The landscape on the plateau is a mixture of short grasses and mid-sized boulders (Figures 4.14 and 4.15). It is an incredibly windy place, where the relentless westerly winds remove most of the annual snowfall from the plateau. Snow drifting occurs along shallow depressions and around rocks and rock piles. Under these conditions SnowTran-3D was able to adequately simulate the snow distribution, and it did capture the major feature by building large drifts on the lee side of the plateau. However, the ratio of observed to modeled snow depth on the plateau (Figure 4.11) reveals the weaknesses of the model. In many areas the model merely removed all of the snow above the determined vegetation snow-holding capacity. Thus, on average the model obtained the correct result by merely blowing all of the snow away. In places where terrain features were resolved by the DEM, the model produced snow drifts which compare well with those observed (transect A in Figure 4.11). These results indicate that more detailed topographic information is required for the model to resolve the smaller features of the observed distribution.

Figure 4.14: Typical January snow distribution on the east side of the Flattop Mountain Plateau looking south towards Long's Peak. This photograph shows snowdrifts occurring along shrubs and small rocks.

Figure 4.15: February 15, 1998 on the Flattop Mountain Plateau. Snow drifts are occurring along small rocky areas and shallow terrain roles.

4.2 Montgomery Pass

4.2.1 Introduction

In the previous two chapters, we examined how SnowTran-3D simulates snow redistribution processes using two different sources of atmospheric forcing data. In Chapter 3 direct meteorological observations were used to drive the model, while in Chapter 4 atmospheric forcing fields were produced by ClimRAMS. In this chapter, we will compare these two methodologies by examining how the simulations conducted for Chapter 4 compare with the observed snow distribution at the Montgomery Pass site. This comparison is possible since the model domains of ClimRAMS and SnowTran-3D encompass the Montgomery Pass site. Again the observed snow distribution on a particular day is used to examine the model's performance.

4.2.2 Experimental Design

The experimental design is essentially identical to the one described earlier in this chapter. The same model simulations (both ClimRAMS and SnowTran-3D) from Chapter 4 were used again here. The important difference is that in the previous section all of the observations used to determine biases in the atmospheric forcing data were from the Flattop Mountain site (the one exception was wind speed). In this Chapter, the model data with corrections for the Flattop Mountain site were applied to the Montgomery Pass site. Thus, this portion of the study evaluates the model and calibration on an independent uncalibrated observation set. The study site is the same one described in Chapter 3, and the same observational transect was used as validation for the model results.

4.2.3 Results

The simulated snow distribution produced by the current methodology is very similar to that produced by the methodology described in Chapter 3. Figure 4.16 shows the simulated snow distribution produced for the Montgomery Pass area. In the below-treeline areas, the annual precipitation never exceeded the vegetation snow- holding capacity; therefore, no snow was available there for transport during the simulation period. In

the above-treeline areas, the vegetation snow-holding capacity was exceeded early in the simulation and snow transport was quite prevalent.

The simulation shows that the windward side of the ridgeline was scoured until less than 0.5 m of snow remained. Since the snow depth in this area exceeded the vegetation snow-holding capacity, the majority of the annual snowfall was removed by wind erosion. The model built a narrow drift band on the lee side, parallel to the ridgeline. Portions of this drift band exceeded 2 m in depth, and the drift depth decreased to the east until reaching the eastern treeline.

The ratio of observed snow depth to the simulated snow depth is displayed in Figure 4.17. The average of this ratio along the observed transect is 1.254. Since this value is close to unity, on average the model did a good job of simulating the snow distribution. However, closer examination of Figure 4.17 reveals that there are sections where the model either over or under predicted the snow depth. To further scrutinize the performance of the model, Figure 4.18 shows a comparison of the observed to modeled snow depth in a profile format. This comparison shows that with the current methodology the model was able to capture the trend in the snow depth changes. The modeled distribution does depict the observed decline from treeline on the west side and its correct location. The peak depth on the lee side is also in the correct location, however, the depth is too shallow by 3 m.

The percent of the annual accumulated snowfall which was returned to the atmosphere during snow transport events was again computed for this area. The computation was completed using the same technique as described in the last two chapters. The amount of mass removed due to sublimation was divided by the amount of snow which fell as precipitation during the simulation period. Figure 4.19 shows a similar pattern as was depicted in Chapter 3 (Figure 3.10). However the sublimation values are higher on the lee side of the ridgeline. Over the ridgeline they are quite similar, although the area where greater than 30% sublimated is slightly larger.

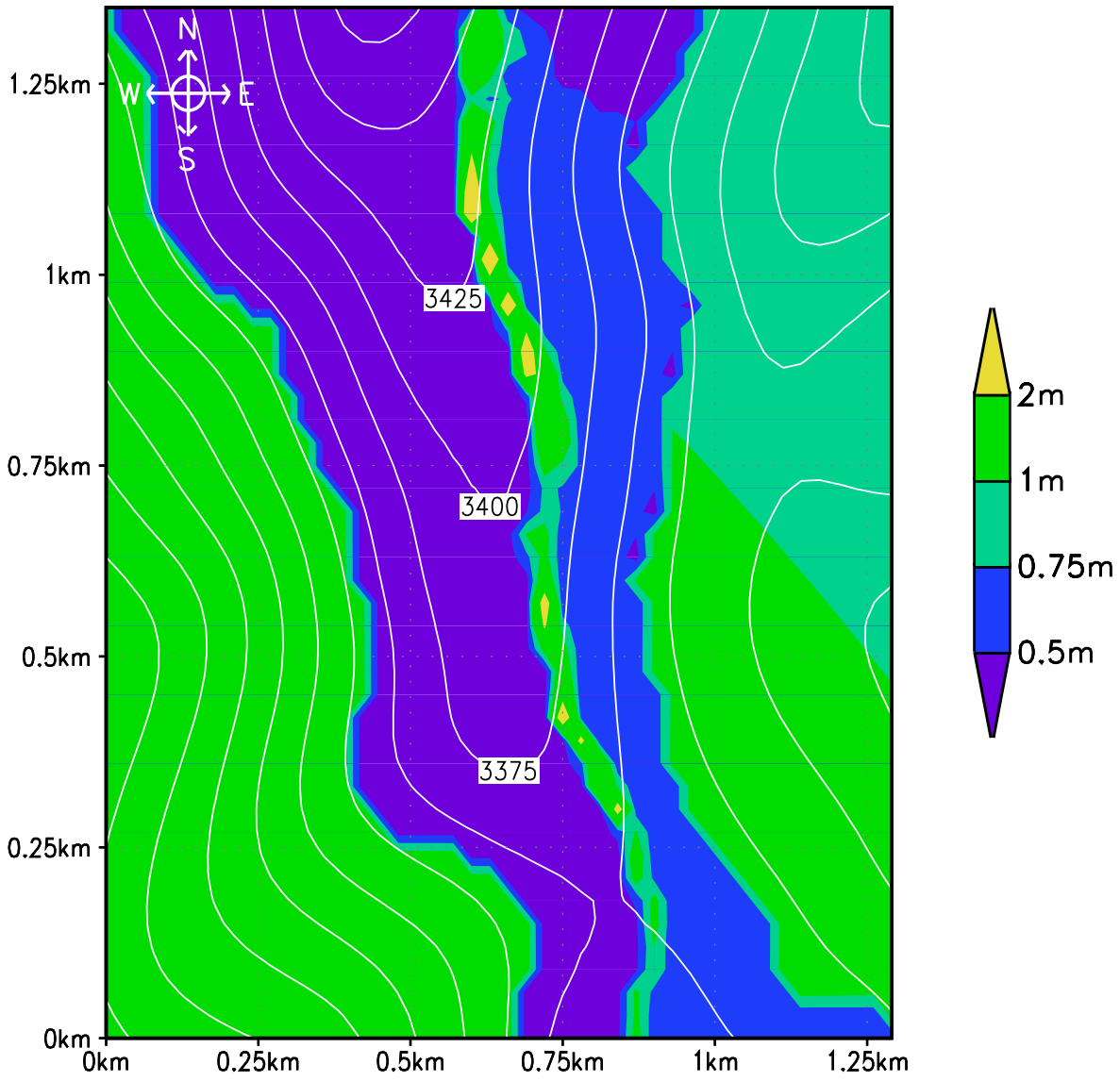

Figure 4.16: Simulated three-dimensional snow distribution for February 15, 1998 produced by SnowTran-3D for the Montgomery Pass Site using ClimRAMS fields as atmospheric forcing data. Contours of topography are in 25 m intervals.

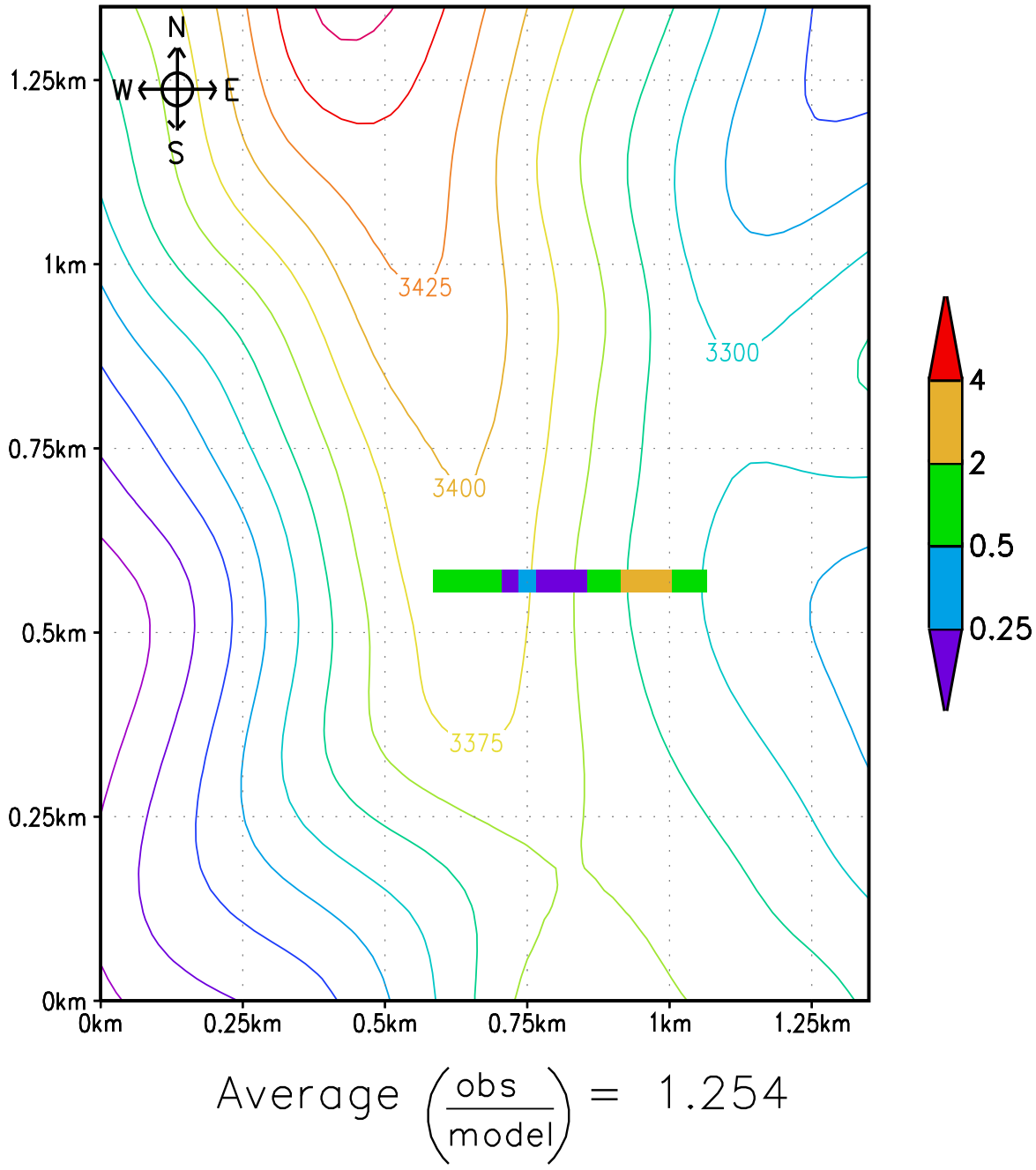

Figure 4.17: Ratio of observed to modeled snow depth along observational transect at Montgomery Pass Site. The observational transect was produced on February 18, 1998. Contours of topography are in 25 m intervals.

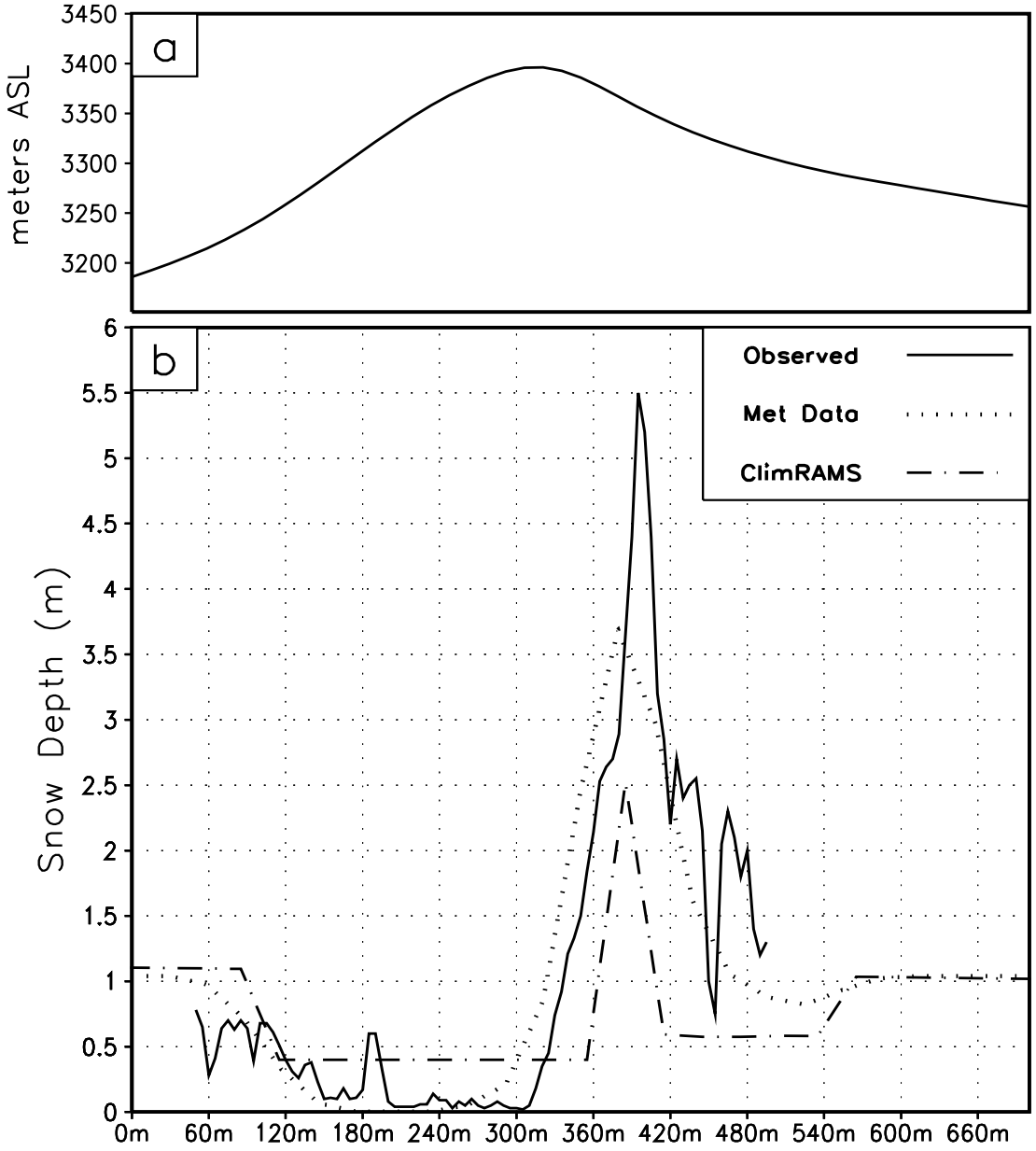

Figure 4.18: a) Model topography along observational transect through Montgomery Pass Site. b) Observed and modeled snow depth along the observational transect. Solid line is the observed snow depth. The dotted line is the snow depth produced by SnowTran-3D when driven by meteorological observations. The dashed line is the snow depth produced by SnowTran-3D when driven by ClimRAMS.

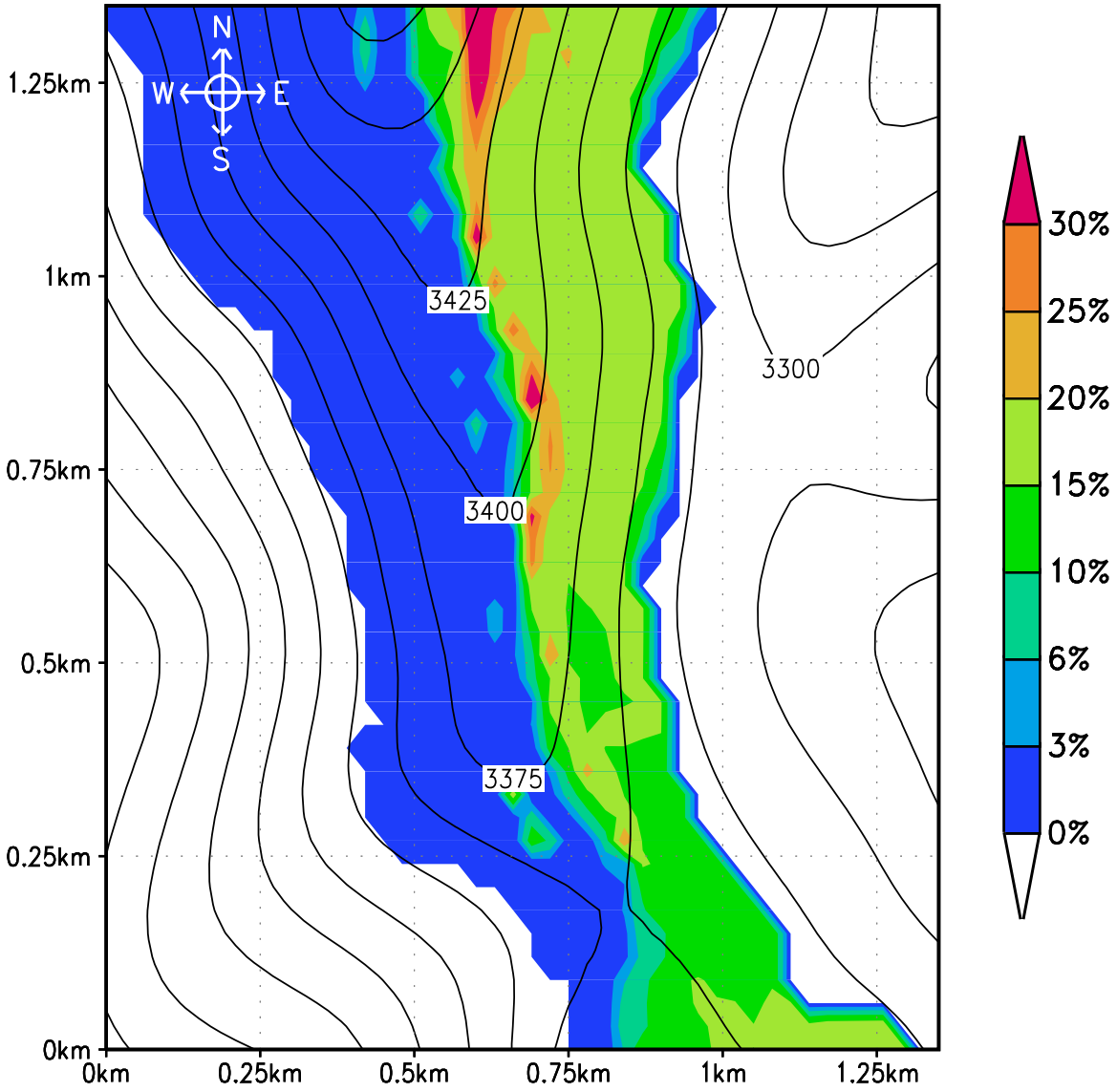

Figure 4.19: Amount of year-to-date precipitation which has been removed due to sublimation of airborne snow at the Montgomery Pass Site. Contours of topography are in 25 m intervals.

4.2.4 Discussion

The simulated snow distribution for the Montgomery Pass site (Figure 4.16) is very similar to the one produced in Chapter 3 (Figure 3.8). Using this methodology, SnowTran-3D was still able to capture the large-scale snow drift features. However, the depth of the snow drifts produced for this chapter is much less than those shown in Figure 4.16. This discrepancy is due to the precipitation inputs for SnowTran-3D. ClimRAMS produced less snow than was observed at the Bear Lake SNOTEL site, and this was accounted for in the adjustment described for the Flattop Mountain Site. However this comparison and adjustment were performed for the Flattop Mountain site, and may not adequately compensate for the amount of precipitation received at the Montgomery Pass site. The simulated drift profile produced in with the current methodology (driving SnowTran-3D from ClimRAMS) is quite similar to the one from Chapter 3 (Figure 4.18). SnowTran-3D was still able to capture the snow distribution: decreasing from treeline into the windward side, and building a lee drift whose depth decreases toward treeline. The snow depth produced with the current methodology is also very similar to the profile from Chapter 3 (Figure 4.18). The main discrepancy is the peak depth of the lee side drift. There is a 1 m difference in this peak, which again was due to the precipitation field being adjusted for a different area.

Figure 4.19 shows the percent of year-to-date precipitation which has been returned to the atmosphere due the sublimation of airborne snow. The pattern produce under the current methodology is quite similar to that produced in Chapter 3. However, the percentages are significantly higher on the lee side of the ridgeline than the values computed in Chapter 3. Sublimation is a highly nonlinear process which depends on air temperature, relative humidity, and wind speed. Hence this discrepancy is due to the combined effects of changes in these atmospheric fields. A partial explanation for the increased sublimation values is portrayed in Figure 4.20. The upper panel shows the observed and modeled air temperatures for the Montgomery Pass Site. Although the model did an excellent job of capturing the synoptic signal, there are several periods where it did not capture the magnitude of the temperature changes. As a result there are several periods where the model

produced air temperatures warmer than those observed. Each one of these periods lasted several days. The lower panel shows the observed and modeled wind speeds. From examining this panel it is evident that during the period where the model produced warmer temperatures, the wind speeds are large enough to facilitate snow-transport. Hence for several multi-day periods, the SnowTran-3D simulation driven by ClimRAMS had warmer temperatures during blow snow events. Due to the increased air temperature during these periods, more sublimation occurred in the ClimRAMS driven simulation.

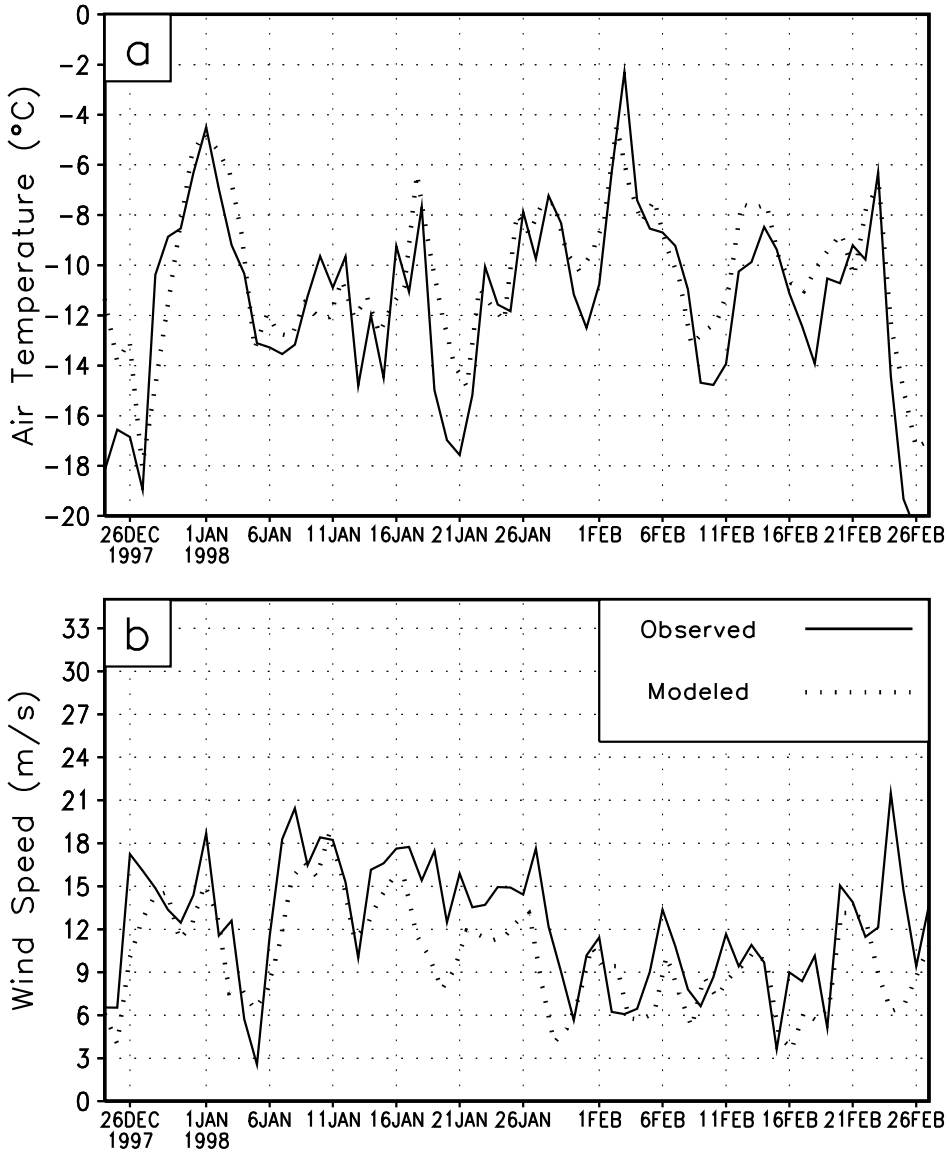

Figure 4.20: a) Observed and modeled air temperature for Montgomery Pass. b) Observed and modeled wind speed for Montgomery Pass. In each panel the observations come from the Montgomery Pass Weather Station. The modeled data comes from the ClimRAMS grid cell which corresponds to Montgomery Pass.

Chapter 5

CONCLUSION

Throughout the course of this study we have examined two methods for driving a snow-transport model. In all cases the snow-transport model used was SnowTran-3D (Liston and Sturm 1998). In Chapter 3, meteorological data collected at a remote weather station were used to drive the snow-transport model, while in Chapter 4 atmospheric fields generated by ClimRAMS were used to drive the snow-transport model. In both cases the snow-transport model was able to capture the large-scale snow distribution features.

The weather at both study sites was characterized by persistent winds with velocities at or above the threshold speed for transport (Schmidt 1980; McClung and Schaerer 1993; Li and Pomeroy 1997). Due to the combined effects of synoptic weather patterns and topography, the dominant wind direction was from the west. This consistent wind direction resulted in the majority of the above-treeline snowpack being eroded from the west side of the ridgeline, and being transported and deposited on the east side.

The one observation missing in each portion of this study was direct precipitation measurements. In each case, precipitation measurements from a near by but lower elevation site were used. Precipitation may be the most important input for determining the seasonal snowcover distribution. Certainly both the final snow distribution and the amount of snow removed due to sublimation are both sensitive to this input. However, it is very difficult to observe the amount of precipitation received at each study site. The strong winds and treeless vegetation which characterize these sites make it nearly impossible to directly measure precipitation on-site.

Currently, daily snow precipitation is measured in two ways for operational use (Doesken and Judson 1996). First by measuring the depth which has been deposited

during a 24 hour period. This depth along with a density measurement produces the snow-water-equivalent (the input needed by SnowTran-3D). The second is to use a gauge which catches and melts snow precipitation and then the snow-water equivalent can be directly measured. Unfortunately both of these techniques are unreliable in the areas where this study took place. Applying either of these methods to alpine sites is difficult due to the prevalence of blowing-snow events. During a blowing snow event it is nearly impossible to distinguish between snow falling as precipitation and snow being transported by wind. Hence the amount captured by a gauge is always generally in error. This also makes measuring the 24 hour depth problematic since the snow is rarely allowed to collect before it is transported by the wind. Brown and Peck (1962) found that gauges in moderately sheltered areas, on average, caught 25% more precipitation than gauges in unsheltered areas. Thus, a suspect measurement is even more suspect.

During the course of this study we have chosen to use SNOTEL observations as precipitation inputs. In each case some adjustment to this data set has been made to account for the elevation differences. Unfortunately, all snow depths and sublimation calculations are sensitive to this input. The snow distribution patterns produced are not nearly as sensitive to the precipitation input. The drift patterns produced by the model in this case are more dependent on the surface characteristics. Throughout the entire study, it was our intention to start with a data set from established measurement rather than attempt to measure the precipitation on site.

In Chapter 3, the model simulated the physical processes associated with the wind-transport of snow, building a drift on the east side of the terrain barrier whose location, mass, width and slope compared well with observations. Given the difference in scales between the model grid and observation interval ($\Delta x_{\text{obs}} = 5$ m, $\Delta x_{\text{model}} = 30$ m) the height of the drift also compared well with the observations. In addition, we expect a higher resolution DEM would have led to improved model simulation. An improved precipitation data set, obtained from a position closer to the research site, would have allowed further scrutiny of the model's sublimation calculations.

In Chapter 4, the model was able to capture the trend in snow distribution along the Flattop plateau. The model built drifts along the lee side of the terrain features resolved

by the model's DEM. Because many of the terrain features which produced drifts were either rock piles or shallow rolls, the model was not able to produce all the observed drift features. A more detailed topographic data set would most likely improve the results obtained in areas dominated by such relatively small-scale terrain features.

An important result obtained in the Flattop Mountain simulations was the building of large drifts along the east-facing cirques off the Continental Divide. Perennial snow fields, such as Andrew's and Tyndall Glaciers, occur in these regions (Outcalt 1965; Outcalt and McPhail 1965). It has been postulated that the presence of these perennial snow fields is due in part to the large amount of snow transport which occurs on the Flattop Plateau. This high elevation plateau catches a large amount of snow during the winter months, and the strong westerly winds move the majority of this snow into the upper reaches of these east facing cirques. The model was able to capture this process and certainly lends credence to this theory.

Blowing and drifting snow, and the snow distributions which these processes create, have relevance to many disciplines. The ability to accurately predict this phenomena can enhance work being done to improve safety and heighten economic goals. Examples of this include, more accurate spring runoff estimates, the capture of snow to improve spring soil moisture conditions for agricultural production, and more accurate avalanche forecasts leading to shorter periods where transportation arteries are closed for control work. In addition, the implementation of a wind and blowing snow model, with the ability to be run in real time, could substantially assist avalanche prediction and control efforts in both the public and private sectors. This study is put forth as an initial demonstration that the tools and techniques required to simulate snow redistribution by wind in complex terrain are now becoming available.

REFERENCES

Auer, A.H., 1974: The rain versus snow threshold temperatures. *Weatherwise*, **27**, 67.

Avissar, R. and Y. Mahrer, 1988: Mapping frost-sensitive areas with a three-dimensional local-scale numerical model Part I: Physical and numerical aspects. *J. Appl. Meteor.*, **27**, 400-413.

Balk, B. and K. Elder, 2000: Combining binary decision tree and geostatistical methods to estimate snow distribution in a mountain watershed. *Water Resources Research*, in press.

Baopu, F., 1995: The effects of orography on precipitation. *Bound.-Layer Meteor.*, **75**, 189-205.

Berg, N.H. 1986: A deterministic model for snowdrift accumulation. *Proceedings of the International Snow Science Workshop*, Tahoe, California, 29-36.

Berg, N., and N. Caine, 1975: Prediction of natural snowdrift accumulation in alpine areas. Final Report to Rocky Mountain Forest and Range Expt. Station (USFS 19-388-CA). Boulder, Dept. of Geography, University of Colorado, 69 pp.

Billings, W.D., 1973: Arctic and alpine vegetations: similarities, differences, and susceptibility to disturbance. *Bioscience*, **23**, 697-704.

Birkeland, K.W. 1997: Spatial and temporal variations in snow stability and snowpack conditions throughout the Bridger Mountains, Montana. Ph.D Dissertation, Arizona State University, p. 161, 168, 174.

Brown, M.J., and E.L. Peck, 1962: Reliability of precipitation measurements as related to exposure. *J. Appl. Meteor.*, **1**, 203-207.

Buser, O., P. Fohn, W. Good, H. Gubler, and B. Salm. 1985: Different methods for the assessment of avalanche danger. *Cold Regions Sci. Tech.*, **10**, 199-218.

Carroll, T.R., 1997: Integrated observations and processing of snow cover data in the NWS hydrology program. *Proceedings, 77th AMS Annual Meeting*, Symposium on Integrated Observing Systems, Long Beach, California, 180-183.

Chen, C., and W.R. Cotton, 1983: A one-dimensional simulation of the stratocumulus-capped mixed layer. *Bound.-Layer Meteor.*, **25**, 289-321.

Chen, C., and W.R. Cotton, 1987: The physics of the marine stratocumulus-capped mixed layer. *J. Atmos. Sci.*, **44**, 2951-2977.

Chiles, J.P., and P. Delfiner, 1999: *Geostatistics: modeling spatial uncertainty.* Wiley, New York, pp. 157-164.

Clark, T.L., and R.D. Farley, 1984: Severe downslope windstorm calculations in two and three spatial dimensions using anelastic interactive grid nesting: A possible mechanism for gustiness. *J. Atmos. Sci.*, **41**, 329-350.

Cline, D.W., 1997: Snow surface energy exchanges and snowmelt at a continental, mid-latitude alpine site. *Water Resources Research*, **33**, 689-701.

Cotton, W.R., J.F. Weaver, and B.A. Beitler, 1995: An unusual summertime downslope wind event in Fort Collins, Colorado, on 3 July 1993. *Wea. Forecasting*, **10**, 786-797.

Cressman, G.P., 1959: An operational objective analysis system. *Mon. Wea. Rev.*, **87**, 367-374.

Daly, C., 1984: Snow distribution patterns in the alpine krummholz zone. *Prog. Phys. Geog.*, **8**, 157-175.

Deardorff, J.W., 1980: Stratocumulus-capped mixed layers derived from a three-dimensional model. *Bound.-Layer Meteor.*, **18**, 495-527.

Deutsch, C.V., and A.G. Journal, 1998: *Geostatistical Software Library and User's Guide.* Oxford University Press, New York, p. 63-94.

Doesken, N.J., and A. Judson, 1996: The snow booklet: A guide to the science, climatology, and measurement of snow in the United States. Colorado State University Department of Atmospheric Science, Fort Collins, CO, 56-71.

Elder, K., J. Dozier, and J. Michalesen, 1991: Snow accumulation and distribution in and alpine watershed. *Water Resources Research*, **27**, 1541-1552.

Evans, B.M., D.A. Walker, C.S. Benson, E.A. Nordstrand, and G.W. Petersen, 1989: Spatial interrelations between terrain, snow distributions and vegetation patterns at an Arctic foothills site in Alaska. *Holarctic Eco.*, **12**, 270-278.

Ferguson, S.A., M.B. Moore, R.T. Marriott, and P. Speers-Hayes, 1990: Avalanche weather forecasting at the northwest Avalanche Center, Seattle, Washington, U.S.A.. *J. Glaciol.*, **36**, 57-66.

Gauer, P., 1998: Numerical snow drift modeling in complex alpine terrain and comparison with field measurements. *Proceedings from the 1998 International Snow Science Workshop.* Sunriver, Oregon, 60-66.

Gesch, D.B., K.L. Verdin, and S.K. Greenlee, 1999: New land surface digital elevation model covers the Earth. *EOS Transactions*, **80(6)**, 69-70.

Gray, D.M., and D.H. Male, 1981: *Handbook of Snow: principles, processes, management, and use.* Pergamon Press, Toronto, p. 380,418.

Harrington, J.Y., 1997: The effects of radiative and microphysical processes on simulated warm and transition season Arctic stratus, Atmospheric Science Paper No. 637.

Department of Atmospheric Science, Colorado State University, Fort Collins, CO. p. 28-76.

Hjermstad, L.M., 1970: Influence of meteorological parameters on the distribution of precipitation across central Colorado mountains. Colorado State University Scientific Paper No. 163, Fort Collins, Colorado.

Isaaks, E.H., and R.M. Srivastava, 1989: *An introduction to applied geostatistics.* Oxford University Press, Oxford, pp. 278-322.

Johnson, G.L., and C.L. Hanson, 1994: Topographic and atmospheric influences on precipitation variability over a mountainous watershed. *J. Appl. Meteor.*, **34**, 68-87.

Kalnay, E., M. Kanamitsu, R. Kistler, W. Collins, D. Deaven, L. Gandin, M. Iredell, S. Saha, G. White, J. Woollen, Y. Zhu, M. Chelliah, W. Ebisuzaki, W. Higgins, J. Janowiak, K.C. Mo, C. Ropelewski, J. Wang, A. Leetmaa, R. Reynolds, R. Jenne, and D. Joseph, The NCEP/NCAR 40-year reanalysis project. *Bull. Amer. Meteor. Soc.*, **77**, 437-471, 1996.

Keyser, D., and R.A. Athens, 1977: The applicability of a mixed-layer model of the planetary boundary layer to real-data forecasting. *Mon. Wea. Rev.*, **105**, 1351-1371.

LaChapelle, E.R., 1980: The fundamental processes in conventional avalanche forecasting. *J. Glaciol.*, **26**, 75-84.

Larson, L.W., 1985: Experiences, investigations and recommendations concerning wind induced precipitation measurement errors. *Workshop on the Correction of Precipitation Measurements*, Zurich, Switzerland, 49-56.

Lee, T.J., 1992: The impact of vegetation on the atmospheric boundary layer and convective storms. Ph.D. Dissertation, Department of Atmospheric Science, Colorado State University, 137 pp.

Liston, G.E. and R.A. Pielke, 1999: A climate version of the Regional Atmospheric Modeling System. *J. Climate*, submitted.

Liston, G.E., and M. Sturm, 1998: A snow-transport model for complex terrain. *J. Glaciol.*, **44**, 498-516.

Liston, G.E., R.L. Brown, and J. Dent, 1993: A two-dimensional computational model of turbulent atmospheric surface flows with drifting snow. *Ann. Glaciol.*, **18**, 281-286.

Liston, G.E., R.A. Pielke, and E.M. Greene, 1999: Improving first-order snow-related deficiencies in a regional climate model. *J. Geophys. Res.*, in press.

Li, L., and J.W. Pomeroy, 1997: Estimates of threshold wind speeds for snow transport using meteorological data. *J. Appl. Meteor.*, **36**, 205-213.

Luce, C.H., D.G. Tarboton, and K.R. Cooley, 1998: The influence of the spatial distribution of snow on basin-averaged snowmelt. *Hydrological Processes*, **12**, 1671-1683.

Mahrer, Y. and R.A. Pielke, 1977: A numerical study of the airflow over irregular terrain. *Beitrage zur Physik der Atmosphare*, **50**, 98-113.

McClung, D., and P. Schaerer, 1993: *The avalanche handbook.* Seattle, The Mountaineers. p 27-30.

McCumber, M.C. and R.A. Pielke, 1981: Simulation of the effects of surface fluxes of heat and moisture in a mesoscale numerical model - Part 1: Soil layer. *J. Geophys. Res.*, **86**, 9929-9938.

McNider, R.T. and R.A. Pielke, 1981: Diurnal boundary layer development over sloping terrain. *J. Atmos. Sci.*, **38**, 2198-2212.

Meyers, M.P., 1995: The impact of a two-moment cloud model on the microphysical structure of two precipitation events. Ph.D. dissertation, Department of Atmospheric Science, Colorado State University, 165 pp.

Meyers, M.P., P.J. DeMott, and W.R. Cotton, 1992: New primary ice nucleation parameterizations in an explicit cloud model. *J. Appl. Meteor.*, **31**, 708-721.

Moore, I., S.D. Mobbs, D.B. Ingham, and J.C. King, 1994: A numerical model of blowing snow around an Antarctic building. *Ann. Glaciol.*, **20**, 341-346.

Naaim, M., F. Naaim-Bouvet, and H. Martinez, 1998: Numerical simulation of drifting snow: erosion and deposition models. *Ann. Glaciol*, **26**, 191-196.

Obleitner, F., and G.J. Mayr, 1996: On the mesoscale structure of the intra-Alpine precipitation distribution during a typical winter snowfall event. *Meteor. Zeischrift*, **5**, 110-120.

Olea, R.A., 1991: *Geostatistical glossary and multilingual dictionary.* Oxford University Press, Oxford, p. 41.

Olienyk, J.P., J.R. Snyder, M.D. Skold, and W.O. Willis, 1979: The economic benefits and costs of managing windblown snow in the Northern Plains of the US. *Proceedings of the Fifth International Conference on Wind Engineering*, July 1979, Fort Collins Colorado, 37-46.

Outcalt, S.I., 1965: The regiem of the Anderw's Glacier in Rocky Mountain National Park, Colorado 1957-1963. *Water Resources Research*, **1**, 277-282.

Outcalt, S.I., and D.D. MacPhail, 1965: A survey of neoglaciation in the Front Range of Colorado. University of Colorado Studies Series in Earth Sciences No. 4. University of Colorado Press, Boulder Colorado.

Perla, R.I., 1970: On contributory factors in avalanche hazard evaluation. *Canadian Geotechnical J.*, **7**, 414-419.

Pielke, R.A., 1974: A three-dimensional numerical model of the sea breezes over south Florida. *Mon. Wea. Rev.*, **102**, 115-139.

Pielke, R.A., 1984: *Mesoscale meteorological modeling.* Academic Press, New York, N.Y., 612 pp.

Pielke, R.A., W.R. Cotton, R.L. Walko, C.J. Tremback, W.A. Lyons, L.D. Grasso, M.E. Nicholls, M.D. Moran, D.A. Wesley, T.J. Lee, and J.H. Copeland, 1992: A comprehensive meteorological modeling system – RAMS. *Meteor. Atmos. Phys.*, **49**, 69-91.

Pomeroy, J.W., D.M. Gray, and P.G. Landine, 1993: The Prairie Blowing Snow Model: characteristics, validation, operation. *J. Hydrology*, **144**, 165-192.

Pomeroy, J.W., and D.M. Gray, 1995: Snowcover accumulation, relocation and management. National Hydrology Research Institute Science Report No. 7, Hydrological Sciences Division, NHRI Division of Hydrology, University of Saskatchewan, Saskatoon, pp 144.

Pomeroy, J.W., P. Marsh, and D.M. Gray, 1997: Application of a distributed blowing snow model to the Arctic. *Hydro. Proc.*, **11**, 1451-1464.

Purves, R.S., J.S. Barton, W.A. Mackaness, and D.E. Sugden, 1998: The development of a rule-based spatial model of wind transport and deposition of snow. *Ann. Glaciol.*, **26**, 196-202.

Rhea, J.O., 1978: Orographic precipitation model for hydrometeorological use. Ph.D. Dissertation, Atmospheric Science Paper No. 287, Department of Atmospheric Science, Colorado State University, 199 pp.

Schmidt, R.A., 1972: Sublimation of wind-transported snow- A model. Res. Pap. RM-90 Rocky Mtn. For. and Range Expt. Sta. For. Serv. U.S. Dept. of Agric., Fort Collins, Colorado.

Schmidt, R.A., 1980: Threshold wind-speeds and elastic impact in snow transport. *J. Glaciol.*, **26**, 453-467.

Schmidt, R.A., 1986: Transport rate of drifting snow and the mean wind speed profile. *Bound.-Layer Meteor.*, **34**, 213-241.

Schmidt, R.A., 1991: Sublimation of snow intercepted by an artificial conifer. *Agric. Forest Meteor.*, **54**, 1-27.

Schmidt, R.A., and H. Hartman, 1986: Storage and redistribution of snow upwind of an avalanche catchment. Proceedings of the International Snow Science Workshop. Tahoe, California, 37-40.

Schultz, P., 1995: An explicit cloud physics parameterization for operational numerical weather prediction. *Mon. Wea. Rev.*, **123**, 3331-3343.

Snook, J.S. and R.A. Pielke, 1995: Diagnosing a Colorado heavy snow event with a nonhydrostatic mesoscale numerical model structured for operational use. *Wea. Forecasting*, **10**, 261-285.

Sturm, M., J. Holmgren, and G.E. Liston, 1995: A seasonal snow cover classification system for local to global applications. *J. Climate*, **8**, 1261-1283.

Sundsbø, P.A., 1997: Numerical modelling and simulation of snow drift. Ph.D Dissertation, The Norwegian University of Science and Technology, Trondheim, Norway; Narvik Institute of Technology, Department of Building Science, Narvik, Norway, pp 112.

Tabler, R.D., 1975: Predicting profiles of snowdrifts in topographic catchments. *Proceedings of the 43rd Annual Western Snow Conference*, San Diego, California, 87-97.

Tremback, C.J. 1990: Numerical simulation of a mesoscale convective complex: Model development and numerical results. Ph.D. dissertation, Atmospheric Science Paper No. 465, Department of Atmospheric Science, Colorado State University, p. 247.

Tremback, C. J., and R. Kessler, 1985: A surface temperature and moisture parameterization for use in mesoscale numerical models. *Preprints, 7th Conference on Numerical Weather Prediction*, 17-20 June 1985, Montreal, Canada, AMS.

Tremback, C.J., G.J. Tripoli, and W.R. Cotton, 1985: A regional scale atmospheric numerical model including explicit moist physics and a hydrostatic time-split scheme. *Preprints, 7th Conference on Numerical Weather Prediction*, June 17-20, 1985, Montreal, Quebec, AMS.

Tripoli, G.J., and W.R. Cotton, 1980: A numerical investigation of several factors contributing to the observed variable intensity of deep convection over south Florida. *J. Appl. Meteor.*, **19**, 1037-1063.

Tripoli, G.J., and W.R. Cotton, 1982: The Colorado State University three-dimensional cloud/mesoscale model - 1982. Part I: General theoretical framework and sensitivity experiments. *J. de Rech. Atmos.*, **16**, 185-220.

Tripoli, G.J., and W.R. Cotton, 1986: Intense, quasi-steady thunderstorm over complex terrain, Pt. 4, Three-dimensional numerical simulation. *J. Atmos. Sci.*, **43**, 894-921.

Uematsu, T., 1993: Numerical study on snow transport and drift formation. *Annals Glaciol.*, **18**, 135-141.

Uematsu, T., Y. Kaneda, K. Tackeuchi, T. Nakata, and M. Yukumi, 1989: Numerical simulation of snowdrift development. *Ann. Glaciol.*. **13**, 265-268.

Uematsu, T., T. Nakata, K. Takeuchi, Y. Arisawa, and Y. Kaneda, 1991: Three- dimensional numerical simulation of snowdrift. *Cold Regions Sci. Tech.*, **20**, 65-73.

Walker, D.A., J.C. Halfpenny, M.D. Walker, and C.A. Wessman, 1993: Long-term studies of snow-vegetation interactions. *BioScience*, **43**, 287-301.

Walko, R.L., W.R. Cotton, M.P. Meyers, and J.Y. Harrington, 1995a: New RAMS cloud microphysics parameterization Part I: the single-moment scheme. *Atmos. Res.*, **38**, 29-62.

Walko, R.L., C.J. Tremback, R.A. Pielke, and W.R. Cotton, 1995b: An interactive nesting algorithm for stretched grids and variable nesting ratios. *J. Appl. Meteor.*, **34**, 994-999.

APPENDIX A: STATISTICAL MAPPING USING ORDINARY KRIGING

Kriging is an geostatistical methodology developed to estimate the distribution of a field when only a limited number of samples are known. This technique is based on empirical work completed by D.G. Krige in South African gold mines (Olea 1991). An attractive feature of kriging is that it starts from a statistical model of nature as opposed to a model of an interpolating function (Chiles and Delfiner 1999). Although this technique was developed for mining applications, during the last twenty years it has been applied to many different disciplines.

Ordinary kriging involves combining a collection of linearized regression relationships in order to minimize an estimation variance. The technique is often described as a "best linear unbiased estimator" (B.L.U.E). Ordinary kriging is best because it strives to minimize the error variance (σ_R^2), it is linear because it utilizes linear regression relationships, and it is unbiased because is attempts to have the mean residual error equal zero ($m_R = 0$). Often it is difficult to maintain these strict criteria since m_R and σ_R^2 are unknown. The kriging method involves building a model of the available data, ensuring that average model error ($\tilde{m}_R$) is exactly zero while minimizing the modeled error variance ($\tilde{\sigma}_R^2$).

In order to examine the development of a kriging model, we will follow the mathematical development discussed in Isaaks and Srivastava (1989). Kriging is developed from a random function model. This approach allows us to express our estimation error as well as its mean value and variance. At each point where the true value of the field is unknown, we estimate the true value using weighted linear combinations of the data available:

$$\hat{v} = \sum_{j=1}^{n} w_j \cdot v \tag{A.1}$$

where v is the true value at that locations and $hatv$ is our estimate. As estimates are produced for values at different locations, the weighting factor is allowed to change. The error in our estimation is defined as the difference between the estimation and the true value ($\text{Error}_i = r_i = \hat{v}_i - v_i$). Therefore the average error of our estimates (m_r) is

$$m_r = \frac{1}{k}\sum_{i=1}^{k} r_i = \frac{1}{k}\sum_{i=1}^{k} \widehat{V}_i - v_i \tag{A.2}$$

However this relationship is not terribly useful since all values of v are unknown.

In order to develop our model, we will look for a probabilistic solution. For our model we will consider the field value at each estimation point (grid box) to be a random variable. Hence each point within our domain (both actual samples and estimations) are outcomes of random variables. The value at each point is a separate stationary random function consisting of several random variables ($V(x_1) \ldots V(x_i)$). The random variable at each location is subject to the same probability law and is denoted as $E[V]$. Since any pair of random variables has a joint distribution which depends on the separation between their two locations, the covariance of the pair is $\widetilde{C}_v(h)$ where h is the distance between the two locations. Since each field value is a random variable, Equation A.1 is a linear combination of random variables and it becomes

$$\widehat{V}\left(x_o\right) = \sum_{i=1}^{n} w_i \cdot V\left(x_i\right) \tag{A.3}$$

and the error

$$R\left(x_0\right) = \widehat{V}\left(x_0\right) - V\left(x_0\right) \tag{A.4}$$

is also a random variable. Equation A.4 will be more useful if it is expressed solely in terms of random variables.

$$R\left(x_0\right) = \sum_{i=1}^{n} w_i \cdot V\left(x_i\right) - V\left(x_0\right) \tag{A.5}$$

As part of our objective to find the best linear unbiased estimation, we desire the error at any and every location to be zero. To do this we apply the formula for the expected value of a linear combination to expression A.5. This formula

$$E\left[\sum_{i=1}^{n} w_i V_i\right] = \sum_{i=1}^{n} w_i E\left[V_i\right] \tag{A.6}$$

enables us to rewrite Equation A.5 as

$$E\left[R\left(x_0\right)\right] = E\left[\sum_{i=1}^{n} w_i \cdot V\left(x_i\right) - V\left(x_0\right)\right] = \sum_{i=1}^{n} w_i E\left[V\left(x_i\right)\right] - E\left[V\left(x_0\right)\right] \tag{A.7}$$

Since the function is stationary, we can write the righthand side in terms of expected values of $V(E[V])$.

$$E\left[R\left(x_o\right)\right] = \sum_{i=1}^{n} w_i E[V] - E[V] \tag{A.8}$$

The expected value of the error at any location is also known as the bias. In order to obtain the best estimation, we desire this error to equal zero.

$$E\left[R\left(x_0\right)\right] = 0 = E[V]\sum_{i=1}^{n} w_i - E[V]$$

$$E[V]\sum_{i=1}^{n} w_i = E[V]$$

$$\sum_{i=1}^{n} w_i = 1$$

This last expression is an additional constraint we place on our system, satisfying it will ensure our solution is unbiased.

The second major component in developing our kriging methodology is to minimize the error variance (σ_R^2). The error variance can be written as

$$\sigma_R^2 = \frac{1}{k}\sum_{i=1}^{k}\left(r_i - m_R\right)^2 = \frac{1}{k}\sum_{i=1}^{k}\left[\hat{v}_i - v_i\frac{1}{k}\sum_{i=1}^{k}\left(\hat{v}_i - v_i\right)\right]^2 \tag{A.9}$$

where $v_1 \ldots v_n$, are the true values of our field and $\hat{v}_1 \ldots \hat{v}_n$, are the estimated values. By assuming that our mean error is equal to zero, Equation A.9 becomes

$$\sigma_R^2 = \frac{1}{k}\sum_{i=1}^{k}\left(r_i - 0\right)^2 = \frac{1}{k}\sum_{i=1}^{k}\left[\hat{v}_i - v_i\right]^2 \tag{A.10}$$

This expression is similar to Equation A.2 in that $\hat{v}$ and v are not always known. However, we can again use random variables to avoid this potential dead end. Again we can write an expression for our estimation as a weighted linear combination

$$\widehat{V}\left(x_0\right) = \sum_{i=1}^{n} w_i V\left(x_i\right) \tag{A.11}$$

Similarly the error is expressed as

$$R(x_0) = \widehat{V}(x_0) - V(x_0) \tag{A.12}$$

The goal of this portion of the development is to minimize the variance of our estimation errors. Since we do not know the actual values of the field, we can not minimize the error in our estimation of these quantities. However, we can minimize the error of our estimation within our model. We do this by finding an expression for the modeled error variance and setting the various partial derivatives to zero.

In order to minimize the variance errors we must first find an expression which represents it. Since the error is a weighted linear combination of random variables, it too is a random variable. The variance of a weighted linear combination can be expressed as

$$Var\left[\sum_{i=1}^{n} w_i \cdot V_i\right] = \sum_{i=1}^{n}\sum_{j=1}^{n} w_i \cdot w_j \cdot Cov\left[V_i V_j\right] \tag{A.13}$$

Utilizing this expression and Equation A.12, we can express the variance of the error as:

$$Var\left[R(x_o)\right] = Cov\left[\widehat{V}(x_o)\,\widehat{V}(x_0)\right] - 2Cov\left[\widehat{V}(x_0)\,V(x_0)\right] + Cov\left[V(x_0)\,V(x_0)\right] \tag{A.14}$$

If we make the assumption that all of the random variables we are utilizing have the same variance, then the last term in Equation A.13 can be rewritten.

$$Cov\left[V(x_0)\,V(x_0)\right] = \tilde{\sigma}^2 \tag{A.15}$$

This allows us to express the error variance as

$$\tilde{\sigma}_R^2 = \tilde{\sigma} + \sum_{i=1}^{n}\sum_{j=1}^{n} w_i w_j \widetilde{C}_{ij} - 2\sum_{i=1}^{n} w_i \widetilde{C}_{i0} \tag{A.16}$$

and once the variance and covariances are known, the error variance becomes a function of n variables (in this case the n variables are the weighting factors). In order to minimize $\tilde{\sigma}_R^2$, we would set its n partial first derivatives equal to zero. However, since our system is still constrained, this operation is not appropriate. The constraint remains because we elected to use unbiased conditions. Therefore we cannot accept any set of n weights as a solution, but must restrict possible solutions to sets of weights whose sum is unity. In order to obtain an unconstrained system we will utilize the Lagrange Parameter technique.

If we attempt to minimize Equation A.16 as an unconstrained system, we will obtain a system of n equations and n unknowns. However, our unbiased condition adds an additional equation leaving us a system of $n+1$ equations and n unknowns. In order to avoid this situation, we may add an additional variable known as a Lagrange Parameter. Of course this parameter must be added so that the equality in A.16 is not disturbed. We can determine what to add to Equation A.16 by examining our unbiased condition.

$$\sum_{i=1}^{n} w_i = 1$$

$$\sum_{i=1}^{n} w_i - 1 = 0$$

$$2\mu \left(\sum_{i=1}^{n} w_i - 1 \right) = 0$$

This last expression can be added to Equation A.16 without disturbing the equality. In this expression, μ is the Lagrange Parameter. With the addition of this last term, our expression for the error variance becomes

$$\tilde{\sigma}_R^2 = \tilde{\sigma} + \sum_{i=1}^{n}\sum_{j=1}^{n} w_i w_j \widetilde{C}_{ij} - 2\sum_{i=1}^{n} w_i \widetilde{C}_{i0} + 2\mu \left(\sum_{i=1}^{n} w_i - 1 \right) \tag{A.17}$$

Now that we have an expression of the error variance in an unconstrained system, we minimize expression A.17 by determining the first order partial derivatives in the equation and setting them equal to zero. We will determine the derivatives of A.17 term by term. For simplicity will take the derivatives with respect to w_1. Expanding the summations in the first term and taking the derivative with respect to the weighting factor yields:

$$\frac{\partial \left(\sum_{i=1}^{n}\sum_{j=1}^{n} w_i w_j \widetilde{C}_{i0} \right)}{\partial w_1} = \frac{\partial w_i^2 \widetilde{C}_{11} + 2w_i \sum_{j=2}^{n} w_j \widetilde{C}_{1j}}{\partial w_1} = 2w_1 \widetilde{C}_{11} + 2\sum_{j=2}^{n} w_j \widetilde{C}_{1j} = 2\sum_{j=1}^{n} w_j \widetilde{C}_{1j}$$

for the second term

$$\frac{\partial \left(\sum_{i=1}^{n} w_i \widetilde{C}_{i0} \right)}{\partial w_1} = \frac{\partial \left(w_1 \widetilde{C}_{10} \right)}{\partial w_1} = \widetilde{C}_{10}$$

and for the third term

$$\frac{\partial\left(\mu\left(\sum_{i=1}^{n} w_i - 1\right)\right)}{\partial w_1} = \frac{\partial\left(\mu w_1\right)}{\partial w_1} = \mu$$

Hence the first derivative of $\tilde{\sigma}_R^2$ with respect to w_1 is

$$\frac{\partial\left(\tilde{\sigma}_R^2\right)}{\partial w_1} = 2\sum_{j=1}^{n} w_j \widetilde{C}_{1j} - 2\widetilde{C}_{10} + 2\mu \tag{A.18}$$

Setting A.18 equal to zero yields

$$\sum_{j=1}^{n} w_j \widetilde{C}_{1j} + \mu = \widetilde{C}_{10} \tag{A.19}$$

Similar equations can be obtained for the different weights, which allows us to write a general expression

$$\sum_{j=1}^{n} w_j \widetilde{C}_{ij} + \mu = \widetilde{C}_{i0} \qquad \text{for } i = 1, \ldots, n$$

This is our ordinary kriging system. This system is often written in matrix form

$$\begin{bmatrix} \widetilde{C}_n & \cdots & \widetilde{C}_{1n} & 1 \\ \vdots & \ddots & \vdots & \vdots \\ \widetilde{C}_{n1} & \cdots & \widetilde{C}_{nn} & 1 \\ 1 & \cdots & 1 & 0 \end{bmatrix} \cdot \begin{bmatrix} 2_1 \\ \vdots \\ w_n \\ \mu \end{bmatrix} = \begin{bmatrix} \widetilde{C}_{10} \\ \widetilde{C}_{n0} \\ \\ 1 \end{bmatrix} \tag{A.20}$$

In order to solve for the weights, we multiply Equation A.20, by the inverse of the C (covariance) matrix.

$$\begin{aligned} &\mathbf{Cw} = \mathbf{D} \\ &\mathbf{C^{-1}} \cdot \mathbf{Cw} = \mathbf{C^{-1}} \cdot \mathbf{D} \\ &\mathbf{w} = \mathbf{C^{-1}} \cdot \mathbf{D} \end{aligned} \tag{A.21}$$

At long last we have a solution. In order to minimize the modeled error variance, we must first determine $(n+1)^2$ covariances which describe the spatial distribution of our random function model. Once this is completed we can build the matrices needed in Equation A.21.

Spline interpolation offers an alternate methodology which could be used for an application similar to the one presented in this study. In order to use spline interpolation, one must postulate a property of the field which is being interpolated. This is very different from kriging where we are modeling the random function. However, utilizing either of these techniques can lead you to an interpolation expression of the same form (Chiles

and Delfiner 1999). In either case, it is important to keep in mind that neither technique explicitly describes the physical processes which produce a distribution. Therefore any structure which appears in the interpolated field and not the data is spurious.

Kriging is a complex technique which can be applied to a wide variety of geostatistical applications. The kriging application contained in this study utilized only the most basic attributes of this technique. For this application, we took a two-dimensional snow depth data set with an observation interval of 50 m and kriged it to the model grid ($\Delta x = \Delta y = 30$ m). This process allowed us to compare the model output to the observations on the same spatial scale. Although the kriging process took a two-dimensional data set and computed a three-dimensional data set, the kriged data are still narrow strips which follow the observational transects. During the kriging process, every attempt was made to minimize the amount of non-observed structure introduced by this process by limiting the search radius of the kriging algorithm. Any structure introduced can be seen in Figure 4.4 as structure within the narrow snow depth bands.